Interplay of reservoirs in a bidirectional system

Ankita Gupta, Bipasha Pal, and Arvind Kumar Gupta*
Department of Mathematics, Indian Institute of Technology Ropar, Rupnagar-140001, Punjab, India

(Received 23 November 2022; accepted 15 February 2023; published 3 March 2023)

Motivated by the interplay of multiple species in several real world transport processes, we propose a bidirectional totally asymmetric simple exclusion process with two finite particle reservoirs regulating the inflow of oppositely directed particles corresponding to two different species. The system's stationary characteristics, such as densities, currents, etc., are investigated using a theoretical framework based on mean-field approximation and are supported by extensive Monte Carlo simulations. The impact of individual species populations, quantified by filling factor, has been comprehensively analyzed considering both equal and unequal conditions. For the equal case, the system exhibits the spontaneous symmetry-breaking phenomena and admits both symmetric as well as asymmetric phases. Moreover, the phase diagram exhibits a different asymmetric phase and displays a nonmonotonic variation in the number of phases with respect to the filling factor. For unequal filling factors, the phase schema can display at most five phases including a phase that shows maximal current for one of the species.

DOI: 10.1103/PhysRevE.107.034103

I. INTRODUCTION

Over decades, there has been a great deal of interest in stochastic transport phenomena of various complex systems such as intracellular transport of cargo vesicles [1,2] and vehicular flow [3,4], both theoretically and physically. Particles either self-driven or driven by some external field traveling stochastically along a one- or multidimensional lattice have been utilized to model various transport processes, both natural as well as man-made [5–8]. In order to analyze the propelled dynamics of these driven diffusive systems, totally asymmetric simple exclusion process (TASEP) is widely used as the most prominent paradigm of the driven models to examine several stationary system features [9–11]. The TASEP model is extensively employed to study the characteristics of various physical systems such as pedestrians [12], vehicular traffic [3], and ants [13], as well as biological systems including movement of motor proteins [14] and protein synthesis [15]. It was originally proposed in 1968 in the context of biopolymerization by ribosomes [16,17]. Since then, this model has served as a discipline of considerable interest to investigate the nonequilibrium behavior of particles moving along a one-dimensional lattice. It studies the collective dynamics of active species, represented by particles that are permitted to enter and exit through the extreme ends of a lattice and hop along a preferred direction in the bulk while considering the hard-core exclusion principle. In such models, the lattice is subject to different boundary conditions which may be either open or periodic. In the case of open boundaries, the steady-state particle density acts as the order parameter and categorizes the phase diagram into three regions, namely low density (LD), high density (HD), and maximal current phase (MC). Moreover, the transition line from LD to HD phase is of the first order and corresponds to a coexistence phase with nonstationary shock, while the transitions from LD to MC and HD to MC phase are of second order with respect to density [11]. If one considers current as the order parameter, all these transitions are of second order. Many complex nonequilibrium phenomena such as shock formation, phase transitions, phase separations, symmetry-breaking, etc., are successfully explained by utilizing this simple model and its several variants [9–11,18–22].

In biological systems, transport of cargoes, viruses, and other information from one particular location to another along microtubules is crucial for the proper functioning of eukaryotic cells [23]. Microtubules are filaments that are directionally polarized with distinguishable plus and minus ends, often serving as a path for many motor proteins, e.g., dynein and kinesin [24]. The movement of motor proteins directed in opposite directions to the extreme ends of the filaments leads to multispecies bidirectional transport. In particular, the kinesin proteins generally travel to the plus end of the microtubule which is away from the nucleus, whereas dyneins tend to walk towards the minus end which is near the nucleus while carrying cargo. This bidirectional flow is not only limited to the biological process but has also been observed in different man-made systems such as vehicular traffic and pedestrian dynamics [3,25,26]. Several attempts have been made focusing on the generalization of the TASEP model from a single-species to a multiparticle system where two different species of particle travel on a lattice in opposite directions. Contrary to the single-species model, these extensions have reported various cooperative phenomena, such as spontaneous symmetry breaking (SSB) and phase separation [22,27–32]. For two different types of propelled particles on a linear path, the "bridge model" was the first model to address the existence of the broken symmetry under analogous

*akgupta@iitrpr.ac.in

dynamical conditions [33]. While the mean-field approach confirms the persistence of one of the asymmetric phases (low-low density phase) to a narrow region, Monte Carlo simulations reveal that this phase may not prevail in the thermodynamic limit [30,34]. Later, this study was extended to analyze multispecies models comprising of two lanes where particles travel in opposite directions and interact only at the boundaries [29,31,35]. However, our understanding of the mechanisms of the SSB phenomenon is very limited [22,27–37].

The majority of the studied TASEP models with open boundaries explore the dynamics of the multispecies system equipped with infinite resources which are far from reality. Many realistic phenomena both physical and biological such as protein synthesis, movement of motor proteins, pedestrian flow, and vehicular traffic involve competition for limited resources on either single or multilane systems. In this direction, several variants of TASEPs have evolved where the entrance rate of the particles is regulated by the occupancy of the reservoir, which leads to an addition of localized shock in the density profile [35,38–52]. In a recent study, a bidirectional system coupled to a finite reservoir has been investigated where the exit rate is also affected by the presence of limited resources [32]. All the research available on such extensions have primarily focused on global constraint on the total number of particles in the system. In a bidirectional system connected to a unified finite reservoir that can hold all the particles, the total occupancy of the reservoir determines the entrance rates of the particles. Circumstantially, a scenario could develop in which the reservoir contains no particle of a certain species and as the entry rates depend upon the total number of particles in the reservoir rather than that of individual species, the dynamics of the system then promote the entry of this species, which is absurd. Several intriguing characteristics could arise if the total particle number of individual species is regulated.

Instigated by the indispensable significance of several reservoirs in a transport process with multispecies systems, the present study examines the dynamics of two particle species moving in opposite directions on a single lattice strategically coupled to two different reservoirs. Our purpose is to investigate the impact of constrained resources for both the species on the stationary properties and characterize its essential features. We attempt to provide a theoretical framework for the system by utilizing mean-field approximation for bidirectional flow on a lattice connected to two reservoirs, each accommodating particles of a single species only. It is interesting to scrutinize the impact of constraints on resources available for each species on the stationary properties of the system, such as the SSB phenomenon and phase separation. Specifically, we aim to address the following queries. (i) How does the presence of finite resources influence the bidirectional flow? (ii) How is the SSB phenomenon affected, when both the particle species are available in equal quantities? (iii) Does the SSB phenomenon still prevail in the case of different capacities of the two reservoirs? (iv) If not, what qualitative and quantitative differences arise in the complex system properties for these two different scenarios?

II. MODEL DESCRIPTION AND THEORETICAL FRAMEWORK

We consider a one-dimensional lattice comprising of L sites identified as $i = 1, 2, \ldots, L$. The boundaries of the lattice are represented by the sites $i = 1$ and $i = L$, whereas the remaining sites are referred to as bulk. Two species of particles denoted by the symbols "+" and "−" translocate on this lattice in opposite directions depicting the bidirectional flow as shown in Fig. 1. The particles interact via the hard-core exclusion principle which guarantees that not more than one particle occupies a single site. In particular, it is assumed that a $+$ particle transverses from left to right, whereas a $-$ particle hops in the reverse direction with a unit rate whenever the adjacent site is empty. If two different species of particles encounter each other on the lattice, they exchange their positions at a rate s, if the direction permits.

Furthermore, it is assumed that the lattice is connected to two finite reservoirs R_+ and R_- having no internal dynamics. The reservoir R_+ can accommodate only $+$ particles, whereas the reservoir R_- solely sustains $-$ particles. The total number of particles of an individual species is taken to be constant in our system. Specifically, N_{t_+} and N_{t_-} quantify the total number of $+$ and $-$ particles, respectively. A $+$ $(-)$ particle from R_+ (R_-) enters the lattice through the site $i = 1$ (L) if empty, with innate entry rate α, hops along the lattice, and then escapes through the site $i = L$ (1) with a removal rate β to rejoin the reservoir R_+ (R_-). As the lattice is coupled to two particle reservoirs, the ingress rate of each species of particle will no longer be constant; instead, it is regulated according to the number of particles in the associated reservoir. Also, a smaller number of particles in the reservoir implies lower entrance rates and enhanced content in the reservoir will lead to an increase in the entrance rates. Therefore, it is reasonable to modify the entrance rate [45] of both species as

$$\alpha^+ = \alpha \frac{N_{r_+}}{N_{t_+}}, \quad \alpha^- = \alpha \frac{N_{r_-}}{N_{t_-}}, \tag{1}$$

where N_{r_+} (N_{r_-}) is the instantaneous number of $+$ $(-)$ particles in the reservoir R_+ (R_-). Clearly, $N_{r_+} \leqslant N_{t_+}$ and $N_{r_-} \leqslant N_{t_-}$ imply that the modified entrance rates remain confined between 0 and α. To scrutinize the effect of coupling the bidirectional transport to two reservoirs, we associate a parameter, namely the filling factor defined as $\mu_j = N_{t_j}/L$, $j \in \{+, -\}$, to each reservoir. Additionally, we define the reservoir quotient as $\rho_{r_j} = N_{r_j}/L$.

To characterize the occupancy status of each site i, we designate two symbols denoted by τ_+^i and τ_-^i, which take binary value 1 in case the site is occupied by $+$ and $-$ particle, respectively, and 0 otherwise. The master equations that govern the dynamics of both the particles in the bulk are given by

$$\frac{d\langle \tau_+^i \rangle}{dt} = J_+^{i-1,i} - J_+^{i,i+1}, \tag{2}$$

$$\frac{d\langle \tau_-^i \rangle}{dt} = J_-^{i+1,i} - J_-^{i,i-1}, \tag{3}$$

where $\langle \cdots \rangle$ represents the statistical average. The terms $J_+^{i-1,i}$ and $J_-^{i+1,i}$ represent the currents in the bulk arising due to

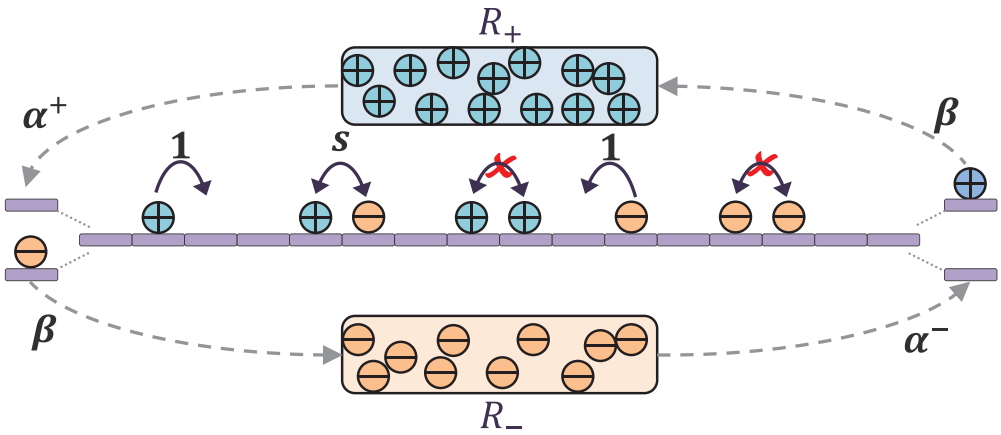

FIG. 1. Schematic diagram for a bidirectional transport model comprised of a lattice connected to two reservoirs, each accommodating particles of a single species only. Blue and red circles denote two oppositely directed particles traveling from left to right and right to left, respectively. The entrance rates of the two particle species are given by α^+ and α^-, which are controlled by the occupancy of the corresponding reservoirs. The exit rates for both the particles is β. Two particles of distinct kinds are permitted to swap their positions with a rate s, if they encounter each other on neighboring sites.

$+$ and $-$ particles, expressed as

$$J_+^{i-1,i} = \langle \tau_+^{i-1}(1-\tau_-^i-\tau_+^i)\rangle + s\langle \tau_+^{i-1}\tau_-^i\rangle, \tag{4}$$

$$J_-^{i+1,i} = \langle \tau_-^{i+1}(1-\tau_-^i-\tau_+^i)\rangle + s\langle \tau_-^{i+1}\tau_+^i\rangle. \tag{5}$$

The first and the second terms on the right-hand sides of the above two equations correspond to the hopping of a particle to the adjacent vacant site and the interchange of the two species of particles in the appropriate direction, respectively. It can be readily seen from Eqs. (4) and (5) that the two bulk current equations are decoupled for $s = 1$ and hence we consider only this case for further study. However, some insight about the scenarios when $s \neq 1$ is given in Sec. V.

For $s = 1$, Eqs. (4) and (5) can be written in simplified form as

$$J_+^{i-1,i} = \langle \tau_+^{i-1}(1-\tau_+^i)\rangle, \quad J_-^{i+1,i} = \langle \tau_-^{i+1}(1-\tau_-^i)\rangle, \tag{6}$$

which implies that a $+$ $(-)$ particle does not distinguish between a hole and a $-$ $(+)$ particle while moving forward. Similarly, the particle evolution equations at the boundaries, $i = 1$ and $i = L$, can be written as

$$\frac{d\langle \tau_+^1\rangle}{dt} = J_+^{\text{enter}} - J_+^{1,2}, \quad \frac{d\langle \tau_+^L\rangle}{dt} = J_+^{L-1,L} - J_+^{\text{exit}}, \tag{7}$$

$$\frac{d\langle \tau_-^1\rangle}{dt} = J_-^{2,1} - J_-^{\text{exit}}, \quad \frac{d\langle \tau_-^L\rangle}{dt} = J_-^{\text{enter}} - J_-^{L,L-1}, \tag{8}$$

where

$$J_+^{\text{enter}} = \alpha^+\langle(1-\tau_+^1-\tau_-^1)\rangle, \quad J_+^{\text{exit}} = \beta\langle\tau_+^L\rangle, \tag{9}$$

$$J_-^{\text{enter}} = \alpha^-\langle(1-\tau_-^L-\tau_+^L)\rangle, \quad J_-^{\text{exit}} = \beta\langle\tau_-^1\rangle. \tag{10}$$

Analyzing Eqs. (2) and (3) along with Eqs. (7) and (8) in the present form is intractable due to the involvement of both one-point and two-point correlators. Therefore, a simple approach known as the mean-field approximation, which has been often used for mathematical treatment in the bidirectional model [22,27,32], is employed. This approximation ignores all kinds of correlations among the particles and the correlator functions are written as a product of individual occupancy numbers, i.e.,

$$\langle \tau_+^i\tau_+^k\rangle = \langle\tau_+^i\rangle\langle\tau_+^k\rangle, \quad \langle\tau_-^i\tau_-^k\rangle = \langle\tau_-^i\rangle\langle\tau_-^k\rangle, \tag{11}$$

where $i, k \in \{1, 2, \ldots, L-1, L\}$. Further, the mean-field densities at site i for particles of either kind are designated as $\rho_+^i = \langle\tau_+^i\rangle$ and $\rho_-^i = \langle\tau_-^i\rangle$. Likewise, the currents corresponding to both particles are written as

$$J_+^{i-1,i} = \rho_+^{i-1}(1-\rho_+^i), \quad J_-^{i+1,i} = \rho_-^{i+1}(1-\rho_-^i). \tag{12}$$

We coarse grain the discrete lattice by introducing a quasi-continuous variable $x = i/L \in [0, 1]$ using the lattice constant $\epsilon = 1/L$ and rescaling time as $t' = t/L$, in the thermodynamic limit. On expanding the mean-field densities in Eqs. (2) and (3) in powers of ϵ and retaining the terms up to the second order, we obtain

$$\frac{\partial\rho_\pm}{\partial t'} = \frac{\partial}{\partial x}\left(\frac{\epsilon}{2}\frac{\partial\rho_\pm}{\partial x} \mp \rho_\pm(1-\rho_\pm)\right). \tag{13}$$

Note that, based on the spatial homogeneity in the continuum limit, the superscript i is dropped. At steady state, the above equation reduces to

$$\frac{\epsilon}{2}\frac{\partial^2\rho_\pm}{\partial x^2} \pm (2\rho_\pm - 1)\frac{\partial\rho_\pm}{\partial x} = 0. \tag{14}$$

In the limit $\epsilon \to 0$, this equation yields $(1-2\rho_\pm)\frac{\partial\rho_\pm}{\partial x} = 0$, i.e., $\frac{\partial J_\pm}{\partial x} = 0$, where $J_\pm$ gives us the bulk current of each species of particle as

$$J_+ = \rho_+(1-\rho_+), \quad J_- = \rho_-(1-\rho_-). \tag{15}$$

Meanwhile, the boundary currents are expressed as

$$J_+^{\text{enter}} = \alpha^+(1-\rho_+^1-\rho_-^1), \quad J_+^{\text{exit}} = \beta\rho_+^L, \tag{16}$$

$$J_-^{\text{enter}} = \alpha^-(1-\rho_-^L-\rho_+^L), \quad J_-^{\text{exit}} = \beta\rho_-^1. \tag{17}$$

As evident from Eqs. (15)–(17), the bulk currents of both species are decoupled and the particle of different kinds effectively interacts only at the boundaries by blocking the entry to

particles of other type. Therefore, the system can be viewed as two independent single species TASEP models coupled only at the boundaries. So, it is reasonable to define the effective entrance rates α_{eff}^{+} and α_{eff}^{-} similar to Refs. [22,27] for the two species of particles by exploiting the continuity of current in bulk and the boundaries of the lattice as

$$\alpha_{\text{eff}}^{+} = \frac{J_+}{\frac{J_+}{\alpha^+} + \frac{J_-}{\beta}}, \quad \alpha_{\text{eff}}^{-} = \frac{J_-}{\frac{J_-}{\alpha^-} + \frac{J_+}{\beta}}. \tag{18}$$

Due to the continuity of current in the bulk, $J_+ = J_+^{\text{enter}} = J_+^{\text{exit}}$ and $J_- = J_-^{\text{enter}} = J_-^{\text{exit}}$. Since the extreme ends of the lattice are coupled to two different finite reservoirs R_+ and R_-, we utilize the particle number conservation condition which gives

$$N_{t_+} = N_{r_+} + N_+, \quad N_{t_-} = N_{r_-} + N_-, \tag{19}$$

where N_+ and N_- denote the number of $+$ and $-$ particles on the lattice, respectively. The above equation can also be rewritten as

$$\mu_+ = \rho_{r_+} + \int_0^1 \rho_+(x)\,dx, \quad \mu_- = \rho_{r_-} + \int_0^1 \rho_-(x)\,dx. \tag{20}$$

Now our objective will be to calculate the effective entrance rates $\alpha_{\text{eff}}^{\pm}$ and the particle densities by utilizing Eqs. (15), (16), and (17) along with Eq. (20). These explicitly obtained expressions for the effective rates will help to quantify the stationary properties of the system such as phase diagrams, density profiles, particle currents, and possible phase transitions.

III. EXISTENCE OF PHASES

To explore the impact of coupling the bidirectional system to separate particle reservoirs corresponding to each species, we study the dynamic properties of the system in the $\alpha - \beta$ parameter space and inspect all the stationary system properties such as density profiles, particle currents, and phase transitions. In literature, the one-dimensional TASEP model for open boundaries with parameters α and β has been reported to exhibit three stationary phases, namely low density (LD), high density (HD), and maximal current (MC) phase [19]. Incorporating constraint on the available resources induces an additional localized shock phase (SP) as a key feature [39,42]. Furthermore, it has been observed that the bidirectional TASEP model with unlimited resources exhibits symmetry-breaking phenomenon [22,27]. Such a model demonstrates two symmetric [i.e., low density (LD-LD) and maximal current (MC-MC) phase] and two asymmetric [i.e., low-low (L-L) and high-low (H-L) phase] phases. In the current model, if the restriction on the available resources is removed, we retrieve the findings for the model with an infinite number of particles [22,27].

Now, let us investigate the feasible stationary phases that might persist in the homogeneous bidirectional TASEP model with two finite particle reservoirs. To clarify, we denote a phase as A-B where A and B illustrate a phase manifest by the $+$ and $-$ particles, respectively. For the proposed model, each species can be found solely in one of the following four phases: low density, high density, maximal current, or shock. We classify the various phases as symmetric or asymmetric based on the nature of their observed stationary properties such as density profiles, effective entrance rates, and particle currents.

A. Symmetric phases

Here, we address the occurrence of various symmetric phases and desire to calculate the explicit effective rates, density profiles, and phase boundaries. For such phases, the two species of particles have identical dynamics as well as stationary properties including effective entrance rates, densities, and currents. In particular, $\mu_+ = \mu_-$, $\alpha_{\text{eff}}^{+} = \alpha_{\text{eff}}^{-}$, $\rho_+ = \rho_-$, and $J_+ = J_-$. Under these circumstances, the effective entrance rates reduce to

$$\alpha_{\text{eff}}^{+} = \frac{\alpha\beta\rho_{r_+}}{\beta\mu_+ + \alpha\rho_{r_+}}, \quad \alpha_{\text{eff}}^{-} = \frac{\alpha\beta\rho_{r_-}}{\beta\mu_- + \alpha\rho_{r_-}}, \tag{21}$$

and in addition from Eq. (20) we acquire

$$\rho_{r_+} = \rho_{r_-}. \tag{22}$$

For the sake of simplification, we designate the common effective entrance rate, filling factor, and reservoir quotient by α_{eff}, μ, and ρ_r, respectively. Our aim is to calculate the effective entrance rates by utilizing the particle conservation criteria to theoretically obtain the expressions for the phase boundaries, shock position, and particle densities.

The system can be thought of as two independent single species TASEP models coupled only at the boundaries, so each species can be found in one of four phases, namely LD, HD, MC, or SP. Keeping in mind the nature of the symmetric phases, only four phases are possible, namely LD-LD, HD-HD, MC-MC, and SP-SP. However, out of these, only two are feasible, specifically LD-LD and MC-MC. The other possibilities such as SP-SP and HD-HD can be discarded based on analytical arguments. Precisely, the HD-HD phase cannot exist as the total particle density cannot be greater than 1. In the case of the SP-SP phase, the constraint $\alpha_{\text{eff}} = \beta$ must be satisfied. However, this condition has no feasible solutions for any value of μ. A summary of the explicit expressions for the existential conditions, effective entrance rates, and the reservoir quotient is given in Table I. The stationary properties, such as particle density, bulk current, reservoir quotient, etc., in each symmetric phase, are detailed in Appendix A.

B. Asymmetric phases

The symmetry of the system is affected by the localized interactions between the distinct particles species at the boundaries, leading to the SSB phenomenon when $\mu_+ = \mu_-$. In the case $\mu_+ \neq \mu_-$, only asymmetric phases exist where the stationary properties of the two species of particles are generally different. Specifically, the densities of the $+$ and $-$ particles in the system are unequal, i.e.,

$$\rho_+ \neq \rho_-, \tag{23}$$

which leads to

$$\alpha_{\text{eff}}^{+} \neq \alpha_{\text{eff}}^{-}. \tag{24}$$

Each particle species can illustrate any of the four phases: low density, high density, shock, or maximal current phase leading

TABLE I. Summary of the existential conditions, effective entrance rates, shock position, and the reservoir quotients for the possible symmetric as well as asymmetric phases for the proposed model. LD-LD and MC-MC represent symmetric phases, while H-L, M-L, S-L and M-M correspond to asymmetric phases. The notations $\alpha^{\pm}_{\rm eff}$ and $\rho_{r_\pm}$ denote the effective entrance rates and the reservoir quotients for the two particle species, whereas x_w gives the position of shock in the S-L phase.

Phase	Phase region/Shock position	$\alpha^{\pm}_{\rm eff}$	$\rho_{r_\pm}$
LD-LD	$\alpha_{\rm eff} < \min\{0.5, \beta\}$	$\mu - \rho_r$	$\frac{\alpha(\mu-\beta)-\beta\mu+\sqrt{4\alpha\beta\mu^2+[\alpha(\mu-\beta)-\beta\mu]^2}}{2\alpha}$
MC-MC	$0.5 < \min\{\alpha_{\rm eff}, \beta\}$	$\frac{\alpha\beta(2\mu-1)}{2\mu(\alpha+\beta)-1}$	$\mu - 0.5$
H-L	$\beta < \min\{\alpha^+_{\rm eff}, 0.5\}$	$\alpha^+_{\rm eff} = \frac{\alpha(\beta-1)\beta^2\rho_{r_+}}{\alpha\rho_{r_+}(\alpha^-_{\rm eff}-1)\alpha^-_{\rm eff}+\beta^2\mu_+(\beta-1)}$	$\rho_{r_+} = \mu_+ - (1-\beta)$
	$\alpha^-_{\rm eff} < \min\{\beta, 0.5\}$	$\alpha^-_{\rm eff} = \frac{\alpha\rho_{r_-}+\mu_- - \sqrt{(\alpha\rho_{r_-}+\mu_-)^2-4\alpha\beta\mu_-\rho_{r_-}}}{2\mu_-}$	$\rho_{r_-} = \frac{1}{2(\alpha+\mu_-)}(\alpha(\mu_- - \beta) + \mu_-(2\mu_- - 1)$ $+\sqrt{[\alpha(\mu_- - \beta) + \mu_-(2\mu_- - 1)]^2 + 4(1-\mu_-)\mu_-^2(\alpha+\mu_-)}\,)$
M-L	$0.5 < \min\{\alpha^+_{\rm eff}, \beta\}$	$\alpha^+_{\rm eff} = \frac{\beta\alpha\rho_{r_+}}{\beta\mu_+ + 4\alpha\rho_{r_+}J_-}$	$\rho_{r_+} = \mu_+ - 0.5$
	$\alpha^-_{\rm eff} < \min\{\beta, 0.5\}$	$\alpha^-_{\rm eff} = \frac{\beta(\mu_- + \alpha\rho_{r_-})}{2\beta\mu_-}$ $-\frac{\sqrt{\beta[\alpha\mu_-\rho_{r_-}+\beta(\mu_- - \alpha\rho_{r_-})^2]}}{2\beta\mu_-}$	$\rho_{r_-} = \frac{1}{8\beta(\alpha+\mu_-)}[\alpha[4\beta(\mu_- - 1) + 1] + 4\beta\mu_-(2\mu_- - 1)$ $+\sqrt{(\alpha[1 + 4\beta(\mu_- - 1) + 4\mu_-\beta(2\mu_- - 1)]^2 - 64\beta^2(\mu_- - 1)\mu_-^2(\mu_- + \alpha))}]$
S-L	$0 \leqslant x_w \leqslant 1$	$\alpha^+_{\rm eff} = \frac{\beta\mu_+ + \alpha\beta\rho_{r_+}}{2\beta\mu_+}$	$\rho_{r_+} = \frac{(\beta-1)\beta^2\mu_+}{\alpha[\alpha^-_{\rm eff}(1-\alpha^-_{\rm eff})+\beta(\beta-1)]}$
	$\alpha^-_{\rm eff} < \min\{\beta, 0.5\}$	$-\frac{\sqrt{\beta[\beta(\mu_+ - \alpha\rho_{r_+})^2 - 4(\alpha^-_{\rm eff}-1)\alpha^-_{\rm eff}\alpha\mu_+\rho_{r_+}]}}{2\beta\mu_+}$	$\rho_{r_-} = \frac{1}{2(\alpha+\mu_-)}(\alpha(\mu_- - \beta) + \mu_-(2\mu_- - 1)$
	$x_w = \frac{\beta+\mu_+-\rho_{r_+}-1}{\alpha^+_{\rm eff}+\beta-1}$	$\alpha^-_{\rm eff} = \frac{\mu_- + \alpha\rho_{r_-} - \sqrt{(\mu_- + \alpha\rho_{r_-})^2 - 4\alpha\beta\mu_-\rho_{r_-}}}{2\mu_-}$	$+\sqrt{\alpha^2(\beta - \mu_-)^2 + \mu_-^2 + 2\alpha\mu_-[\beta + \mu_-(1-2\beta)]})$
M-M	$0.5 < \min\{\alpha^+_{\rm eff}, \beta\}$	$\alpha^+_{\rm eff} = \frac{\alpha\rho_{r_+}}{\beta\mu_+ + \alpha\rho_{r_+}}$	$\rho_{r_+} = \mu_+ - 0.5$
	$0.5 < \min\{\alpha^-_{\rm eff}, \beta\}$	$\alpha^-_{\rm eff} = \frac{\alpha\rho_{r_-}}{\beta\mu_- + \alpha\rho_{r_-}}$	$\rho_{r_-} = \mu_- - 0.5$

to the total number of possible asymmetric phases displayed by the system being equal to $4^2 = 16$. Keeping in view that the total particle density is bounded above by 1, phases such as M-H, H-M, S-M, M-S, H-S, S-H, and H-H are discarded. The S-S phase can be eliminated based on mathematical argument. Now, to calculate the effective entrance rates for the remaining eight feasible phases, we need to determine the reservoir quotients by utilizing the particle number conservation for each species. These expressions will be further employed to obtain the phase boundaries, the position of shock, and the particle densities. Table I summarizes the existence criteria, effective entrance rates, the position of shock, and the reservoir quotients for each possible asymmetric phase. The theoretical computation for the expressions of each phase in this category is explained in Appendix B.

We have obtained the explicit theoretical expressions for the stationary particle densities, phase boundaries, and reservoir quotients for each feasible phase by employing a mean-field approach. Additionally, the steady-state particle densities can also be procured from Eq. (13) along with the boundary conditions given by Eqs. (16) and (17) numerically by utilizing a finite difference scheme outlined in Appendix C. Although the approach is simple to use, the theoretical phase boundaries cannot be obtained through this method, making it difficult to conduct a thorough analysis of how different parameters, such as the filling factors, affect the stationary features of the system.

IV. RESULTS AND DISCUSSION

In this section, we inquire about the effect of coupling the system with two finite reservoirs on the steady-state properties and obtain the phase diagrams for specific values of μ_+ and μ_- in the parameter space $\alpha - \beta$. We perceive both qualitative and quantitative changes in the topology of the phase diagram specifically in terms of symmetry breaking for $\mu_+ = \mu_-$ and the emergence of other phases. The theoretical outcomes obtained in the previous section involve several approximations; therefore, to validate these results, we perform elementary Monte Carlo simulations following the random-sequential update rule for $2 \times 10^7 L$ time steps. At each simulation step, a site is chosen randomly, upon which the dynamic rules described in Sec. II are implemented. The initial 5% of the time steps are scraped ensuring the system reaches a steady state. We segregate our further analysis into two distinct categories: (i) when the filling factors are symmetric, $\mu_+ = \mu_-$, and (ii) when the filling factors are asymmetric, $\mu_+ \neq \mu_-$.

A. Symmetric filling factor ($\mu_+ = \mu_-$)

Motivated by the findings of a bidirectional TASEP model with a single infinite reservoir where symmetry-breaking phenomena have been observed, we wish to study a constrained system where the number of particles of both species is equal. To simplify, we prefer to refer to the common filling factors by μ. Initially, for a very small value of μ, the phase

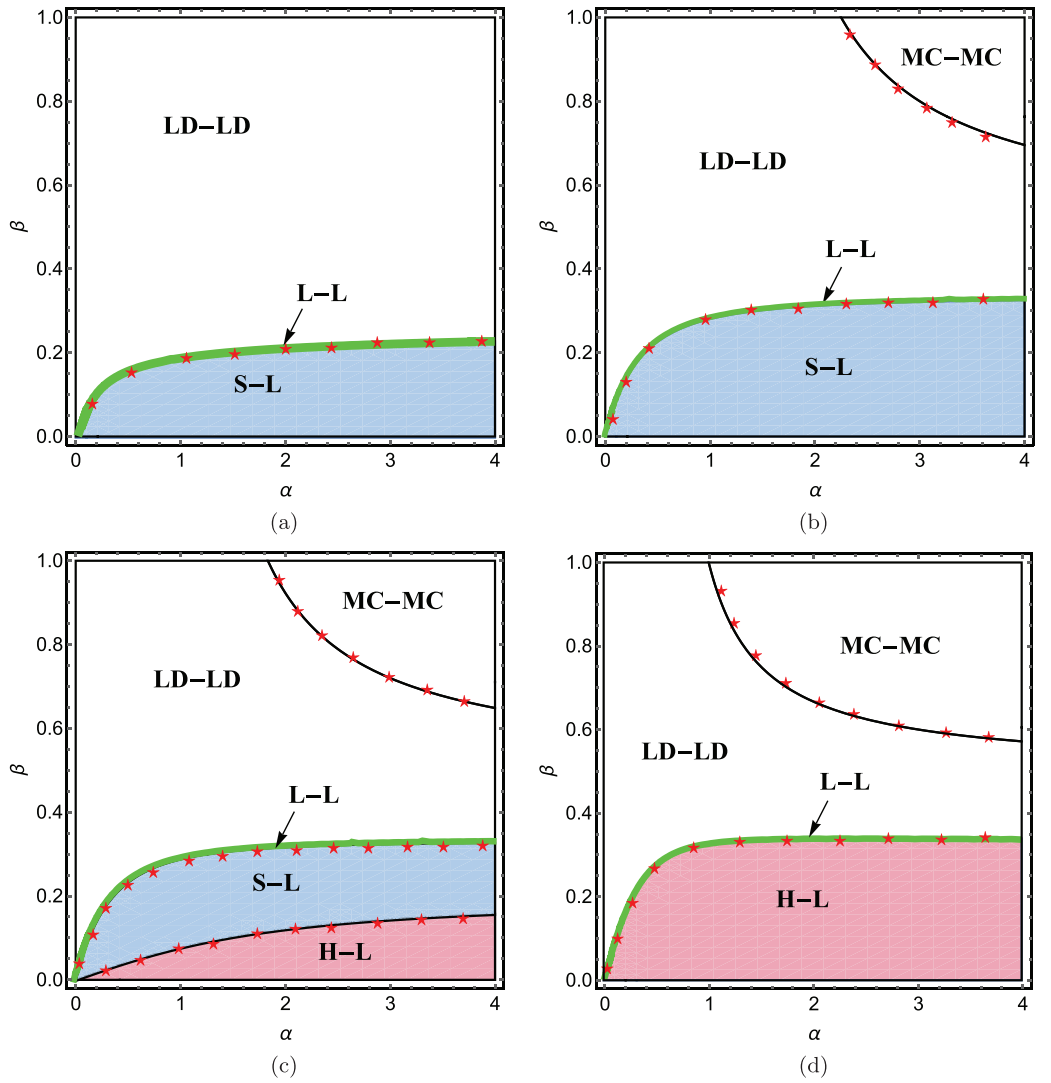

FIG. 2. Stationary phase diagrams for (a) $\mu = 0.3$, (b) $\mu = 0.9$, (c) $\mu = 1.1$, and (d) $\mu = 100$. Symmetric phases are represented by white regions, while the colored regions denote asymmetric phases. Red symbols correspond to Monte Carlo simulation results. The L-L phase remains confined to a curve and acts as a boundary separating H-L and LD-LD phases, displaying a first order phase transition taking average current as the order parameter. The size of the system is taken to be 1500.

diagram is comprised of one symmetric phase namely LD-LD as presented in Fig. 2(a) for $\mu = 0.3$. Despite the symmetry in the dynamic rates of both $+$ and $-$ particles, the system reveals two asymmetric phases: S-L and L-L. The stationary characteristics of the two species vary in such phases. It is noteworthy to specify that symmetry-breaking phenomenon is observed in the system even when the total number of particles of each species is much less. Moreover, the L-L phase remains confined to a curve forming a boundary separating the LD-LD and the S-L phase regions. No substantial changes are observed in the phase schema until $\mu = 0.5$, except for the expansion of the S-L and shrinkage in the LD-LD region. With the enhancement in μ from 0.5, another symmetric phase namely MC-MC appears in the phase diagram in addition to the previously existing phases, which is evident from Fig. 2(b) for $\mu = 0.9$. This appearance of a symmetric maximal current phase after $\mu = 0.5$ is affirmed by Eqs. (A6) and (A7). At this stage, adequate particles are available to fill the lattice entirely and retain the MC-MC phase.

With the further advent in μ, no other symmetrical phase is observed. As soon as $\mu > 1$, an asymmetric phase precisely H-L enters the phase schema next to the S-L phase, resulting in the shrinkage of the later mentioned phase region [as prescribed in Fig. 2(c)]. It can also be guaranteed from Eq. (B5) that a necessary condition for the existence of H-L is $\mu > 1$. Further increasing the value of μ results in the expansion of the H-L phase region and, as $\mu \to \infty$, the S-L phase disappears altering the topology of the phase diagram both qualitatively and quantitatively. Note that, in the extreme case of $\mu \to \infty$, the rates α^+ and α^- approach the innate entrance rates and the global limitation on the number of particles is bygone. As expected, the system behaves as a bidirectional two species model with infinite resources where two symmetric phases, LD-LD, MC-MC, and two asymmetric phases, L-L and S-L persist [22,27]. Clearly, the number of observed phases in the stationary phase diagrams changes from $3 \to 4 \to 5 \to 4$ as μ increases, displaying a nonmonotonic trend.

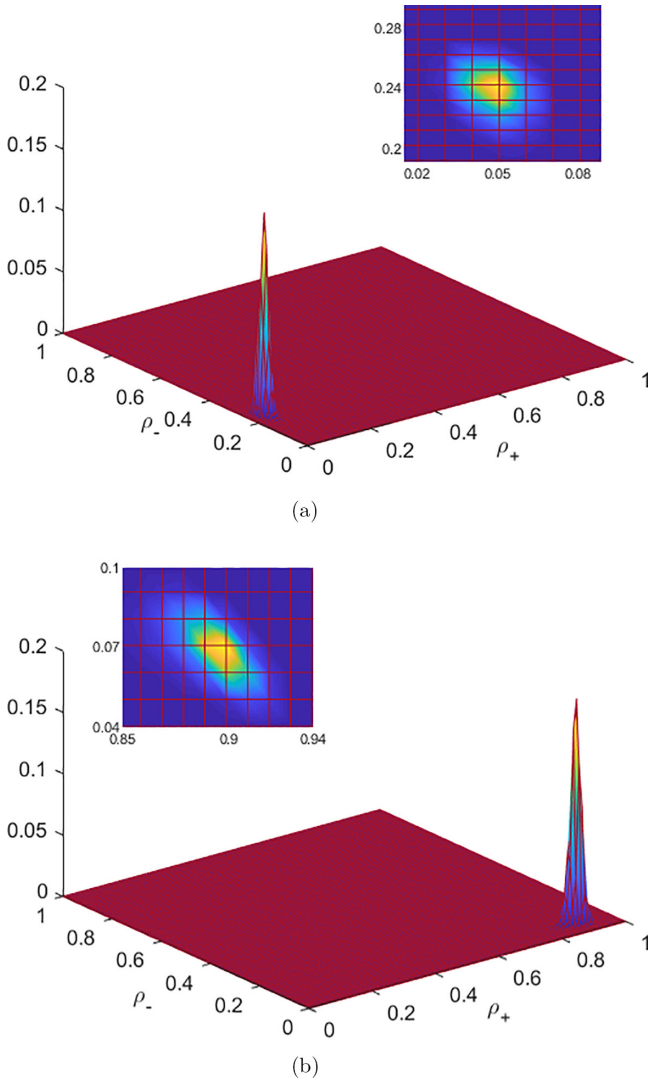

FIG. 3. Particle density histogram for (a) L-L and (b) H-L phases with the parameters $(\alpha, \beta, \mu) = (1, 0.1, 0.3)$ and (2,0.1,1.5), respectively. Insets show the two-dimensional contour plot.

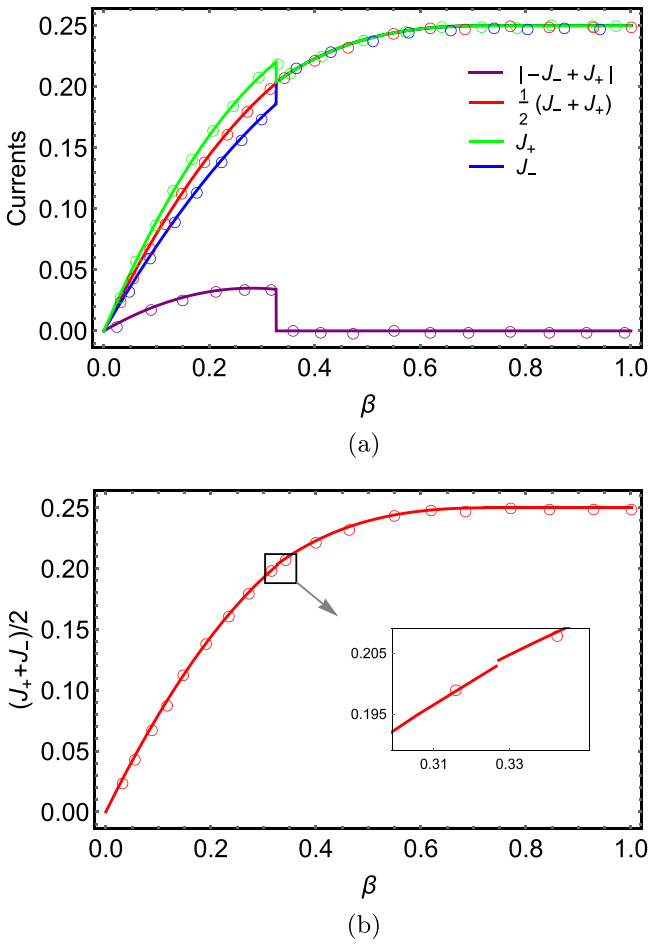

FIG. 4. Plot of currents (a) $(J_+ + J_-)/2$, $|J_+ - J_-|$, J_+, and J_- and (b) $(J_+ + J_-)/2$ vs β for $\alpha = 3$ and $\mu = 1.1$. Inset in (b) displays a discontinuity in $(J_+ + J_-)/2$ near $\beta \approx 0.326$. Solid lines represent theoretical results and symbols refer to Monte Carlo simulations.

1. Spontaneous symmetry-breaking phenomenon (SSB)

One of the most remarkable features of a bidirectional system is the spontaneous symmetry-breaking phenomenon. To investigate this occurrence in detail through Monte Carlo simulations, we generate particle density histograms by continuously monitoring the instantaneous particle densities ρ_+ and ρ_- of the positive and the negative species. In simulations, considering a system size of $L = 1000$, initial 10^9 time steps are discarded and then we gather data for 9×10^9 time steps. If the peak in the density histogram distribution satisfies $\rho_+ = \rho_-$, the corresponding phase is labeled as symmetric; otherwise, it is labeled as an asymmetric phase. Figure 3 shows the typical density histogram plots for L-L and H-L phases in the case of the symmetric filling factor with $(\alpha, \beta, \mu) = (1, 0.1, 0.3)$ and (2,0.1,1.5), respectively. In the case of the L-L phase, Fig. 3(a) demonstrates that a peak occurs for $\rho_+ < \rho_- < 0.5$, which means that the symmetry breaking is observed. For the H-L phase, as anticipated, a peak with $\rho_+ > 0.5$ and $\rho_- < 0.5$ is obtained as shown in Fig. 3(b).

The SSB phenomenon can also be analyzed by inspecting the nature of the currents corresponding to the two species of particles as well as the possible phase transitions for a chosen set of parameters. The currents J_+ and J_- when plotted with respect to β for $\alpha = 3$ with filling factor $\mu = 1.1$, as shown in Fig. 4(a), display a sudden change at the value $\beta \approx 0.326$ after which they remain equal. To investigate this observation in detail, we further plot the value of the currents $(J_+ + J_-)/2$ and $|J_+ - J_-|$ for $\alpha = 3$ and $\mu = 1.1$. The average particle current in the system along the line $\alpha = 3$ also displays similar behavior near the critical point $\beta \approx 0.326$ [see Fig. 4(b)]. This abrupt change is a consequence of the transition from symmetric to asymmetric phases. Moreover, the behavior of $|J_+ - J_-|$ also changes at the point $\beta \approx 0.326$, after which it remains constant and takes the value zero, confirming the emergence of the symmetric phase. Note that the phase diagram for $\mu = 1.1$ given by Fig. 2(c) illustrates a phase transition from asymmetric to symmetric phases as S-L $\rightarrow$ H-L $\rightarrow$ L-L $\rightarrow$ LD-LD $\rightarrow$ MC-MC as β varies. Further, when the particle currents for each species are individually analyzed, it can be noted that the current associated with the $+$ particles is greater than or equal to the current associated with the $-$ particles [see Fig. 4(b)]. Mathematically, the existential conditions given by

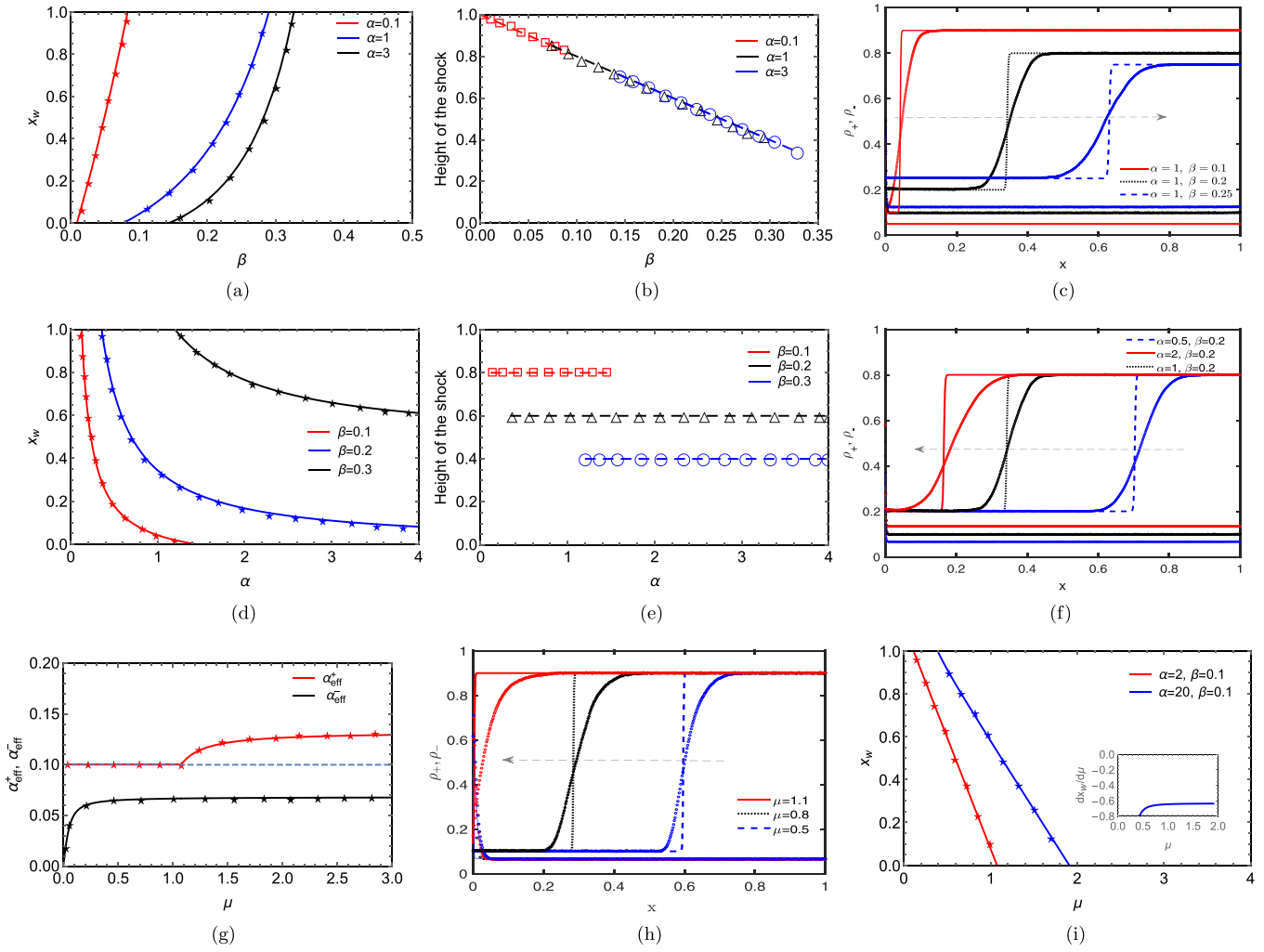

FIG. 5. (a), (b) Position and height of the shock with respect to β for $\mu = 1.1$ and $\alpha = 0.1,\ 1,\ 3$. (c) Density profiles for fixed $\alpha = 1$ and $\beta = 0.1,\ 0.2,\ 0.25$ with $\mu = 1.1$. (d), (e) Position and height of the shock with respect to α for $\mu = 1.1$ and $\beta = 0.1,\ 0.2,\ 0.3$. (f) Density profiles for fixed $\beta = 0.2$ and $\alpha = 0.5,\ 1,\ 2$ with $\mu = 1.1$. (g) Effective entrance rates with respect to μ for $\alpha = 2$ and $\beta = 0.1$. (h) Density profiles for $\alpha = 2$ and $\beta = 0.1$ for $\mu = 0.5,\ 0.8,\ 1.1$. (i) Position of the shock with respect to μ for $\alpha = 2,\ 20$ and $\beta = 0.1$. Inset shows the change in position of the shock with respect to μ for $\alpha = 20$ and $\beta = 0.1$. In all figures, solid lines represent theoretical results and symbols correspond to Monte Carlo simulations. The size of the lattice is taken to be 3000.

Eqs. (B5) and (B12) of H-L and S-L phases, respectively, require the effective entrance rate of the negative species to remain lower than the exit rate implying that the current $J_- = \alpha^-_{\rm eff}(1 - \alpha^-_{\rm eff})$ is less than the current $J_+ = \beta(1 - \beta)$. Thus one can conclude that the transition from asymmetric phases to symmetric phases with respect to current is of the first order.

2. *Shock dynamics*

We now discuss the features of the localized shock that appears in the density profile of the asymmetric S-L phase. In the thermodynamic limit, Eq. (13) reduces to the continuity equation given by $\partial\rho_\pm/\partial t' \pm \partial J_\pm/\partial x = 0$ and the speed of shock for $+$ species is expressed as $s = \beta - \alpha^+_{\rm eff}$. For the existence of shock, its speed in the corresponding lattice must be equal to zero. Using this condition, as well as the particle number conservation, the steady-state properties of the S-L phase have been thoroughly investigated and details are provided in Appendix B.

Now, we focus on the propagation of shock with respect to the exit rate as well as the entry rate using the analytical expression of shock position given by Eq. (B11), which is detailed in Appendix B. From Fig. 5(a) and Fig. 5(c), one can observe that upon the variation of exit rate, the shock position changes continuously from 0 to 1. It means that, with an increase in β after a certain critical value, marking the phase boundary S-L and H-L, the shock enters the lattice from the left end. Further increase in β shifts the shock towards the right until it attains the value corresponding to the phase boundary between S-L and L-L, beyond which the shock leaves the lattice. In this case, the nonzero shock height, which depends solely on β, decreases linearly [see Fig. 5(b)]. Similarly, upon varying the entry rate, the position of shock displays a shift from the right end towards the left end [see Fig. 5(d) and Fig. 5(f)]. The height of this shock remains constant throughout the variation of entry rate due

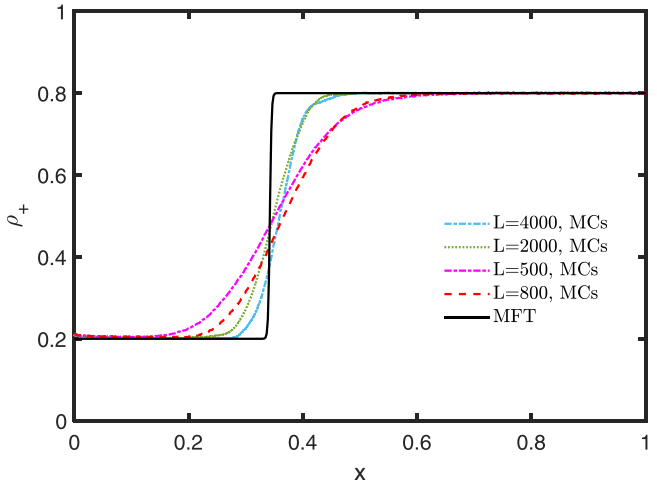

FIG. 6. Effect of finite lattice length L on the S-L profile for fixed $(\alpha, \beta, \mu) = (1, 0.2, 1.1)$ and varied values of L.

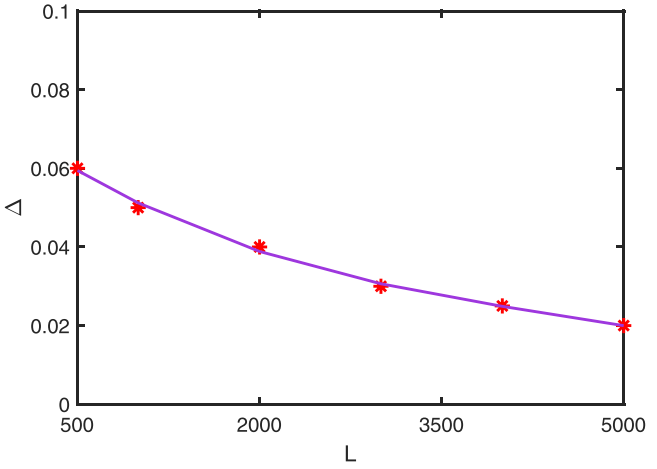

FIG. 7. Region width (Δ) of low-low density (L-L) phase with respect to β for fixed $\alpha = 0.5$ and $\mu = 0.5$. The solid curve is a guide to the eye with best-fit polynomial for the discrete simulation data (shown by red markers) until $L \approx 5000$.

to dependence on β that remains fixed [see Fig. 5(e)]. Thus, if one considers the position and height of shock as order parameters, then the transitions are of second and first order, respectively.

The localized shock appears as a consequence of finite resources; therefore, it is imperative to understand how the filling factor impacts the propagation of shock. In this regard, we choose a point from $\alpha - \beta$ space and analyze the impact of varying μ on the properties of shock. Due to the dependence of shock height only on β, one can readily conclude that it remains constant with respect to μ. This subsequently means that α^+_{eff} remains constant throughout the S-L phase. However, α^-_{eff} is found to increase. To support these analytical arguments, we have plotted the effective rates in Fig. 5(g) and Fig. 5(h). Moreover, from Fig. 5(h) one can observe that the shock shifts towards the right end with respect to μ for constant (α, β) until it reaches the left end and finally leaves the lattices. This signifies the transition from S-L to H-L phase that appears as a consequence of the effective entry rate exceeding the exit rate for $+$ species [see Fig. 5(g)]. To validate it mathematically, the effective rates for both the species have been calculated in the limit $\mu \to \infty$ and are given as

$$\alpha^+_{\text{eff}} \to \frac{2\alpha\beta^2(\beta-1)}{\alpha^3 + 2(\beta-1)\beta^2 - \alpha^2[2\beta - 1 + \sqrt{(1+\alpha)^2 - 4\beta\alpha}]} \tag{25}$$

and

$$\alpha^-_{\text{eff}} \to \frac{1+\alpha-\sqrt{(1+\alpha)^2-4\alpha\beta}}{2}, \tag{26}$$

which satisfies the existential conditions for the H-L phase. Furthermore, the shift in position is predominantly linear for higher values of μ, which can be viewed from Fig. 5(i) where the derivative approaches a linear profile with an increase in μ.

3. Finite size effect on asymmetric phases

It has been observed in past studies that TASEP with symmetry breaking phenomenon results in rigorous size-scaling dependencies [27,33]. So, to further analyze this effect of the finite lattice length L on the shock-low density phase in the proposed model, we have plotted the density profiles for a point $(\alpha, \beta) = (1, 0.2)$ chosen in the S-L region with $\mu = 1.1$ for different values of L (see Fig. 6). As anticipated, the shock profile is primarily sharpened by an increase in the value of L, while the underlining S-L phase remains intact.

The other asymmetric phase, L-L, arises in the system even for a relatively small number of particles of each species and persists for its higher value, as illustrated in Fig. 2. According to the mean-field approximation, this phase exists on a curve while simulations reveal that it appears for a considerable domain, as also reported earlier [29,30]. To study this effect of the system size on the L-L phase, we plot the region width (Δ) with respect to β for fixed $\alpha = 0.5$ and $\mu = 0.5$ in Fig. 7. As observed from the figure, the region width Δ decreases with an increase in L and almost shrinks to a restricted range at $L \approx 5000$. We have plotted $\Delta(L)$ with best-fit polynomial as a guide to the eye for the discrete simulation data in Fig. 7. As expected, based on simulations, the L-L phase region exists for a significant range of β for smaller values of L, while, for larger system size, it shrinks to a narrow region, thereby substantiating the theoretical observations in the thermodynamic limit.

B. Asymmetric filling factors ($\mu_+ \neq \mu_-$)

Now let us inquire into the bidirectional system when the filling factors corresponding to the two species of particles are distinct. Even if both the particle species demonstrate the same phase, all their stationary properties cannot be equal, specifically, the particle density, and therefore there is no point in talking about the SSB phenomenon in this case. The difference in the filling factor forces the system to manifest only asymmetric phases. Without loss of generality, we choose to discuss the crucial properties such as the density profiles, phase diagrams, and phase transitions for the case when $\mu_+ > \mu_-$. The reverse scenario where $\mu_+ < \mu_-$ can be investigated from the results attained for $\mu_+ > \mu_-$ by utilizing the transformations discussed at the end of this section.

To explore the impact of coupling the system with two different reservoirs on the stationary properties, we analyze our system in two distinct cases: (i) taking fixed small, intermediate, or large values of μ_-; simultaneously varying μ_+ and (ii) fixing μ_+ and changing values of μ_-.

1. Stationary properties: Impact of μ_+

Here, we aim to focus on the structural variations that occur in the phase diagram when μ_- is kept fixed and the filling factor corresponding to positive particles μ_+ changes. For the case when both the filling factors were equal, our discussion in Sec. IV A reveals that important topological changes were encountered in the phase diagram at critical points $\mu = 0.5$ and 1. Therefore, we consider three different circumstances: $\mu_- \leqslant 0.5$, $0.5 < \mu_- \leqslant 1$, and $1 < \mu_-$.

When the filling factor μ_- is kept less than $\min\{0.5, \mu_+\}$, varying the other filling factor strongly influences the stationary phase diagram as presented in Fig. 2(a) and Fig. 8 for $\mu_- = 0.3$. Initially, when $\mu_+ = \mu_-$, three phases were observed comprising one symmetric (LD-LD) and two asymmetric phases (L-L and S-L). As soon as $\mu_+ \neq \mu_-$, the LD-LD phase disappears because the system no longer satisfies symmetric conditions for the rates. This phase is substituted by the asymmetric L-L phase where the particle densities of the two species are dissimilar. The vanishing of the symmetric phases also indicates the termination of the SSB phenomena. As μ_+ increases beyond 0.5, two phases, M-L and H-L, emerge in the phase schema; see Fig. 8(a). On further increment in μ_+, the regions for M-L and H-L grow in size. This expansion is attributed to the fact that, with increasing μ_+, the particle flux of the positive species becomes larger while the flux of the negative species remains unaltered. As $\mu_+ \to \infty$, the S-L phase is no longer realized, along with H-L and M-L covering the majority of the phase diagram [see Fig. 8(b)]. Note that the number of phases with respect to μ_+ changes from three to four and then reduces to three, which depicts a nonmonotonic trend.

We now concentrate on the stationary properties of the system when μ_- satisfies $0.5 < \mu_- \leqslant \mu_+$. The outcomes of the theoretical analysis and Monte Carlo simulations are presented in Fig. 9 for $\mu_- = 0.9$ and different values of μ_+. There are four phases in the system for $\mu_+ = \mu_- = 0.9$ [see Fig. 2(c)] among which LD-LD and MC-MC are the phases which are the most sensitive to the change in the value of μ_+. These phases are replaced with L-L and M-M phases for $\mu_+ \neq \mu_-$ along with the introduction of the maximal-low (M-L) region into the phase representation. The persistence of asymmetric maximal-low phase requires either one of μ_+ or μ_- must be greater than 0.5. The corresponding topological structure of the phase diagram is illustrated in Fig. 9(a). It is important to note that, though the bulk characteristics of the two particle species are the same in both MC-MC and M-M phases, the particle densities are not equal at the boundaries. Specifically, the effective entrance rates are different in cases of M-M [as confirmed from Eq. (24)] implying that $\rho_+(0) \neq \rho_-(1)$. Now, as μ_+ increases, the H-L phase enters the phase diagram next to the S-L phase when $\mu_+ > 1$ [see Fig. 9(b)]. This critical point after which H-L appears in the phase schema is obtained from the condition that the existence

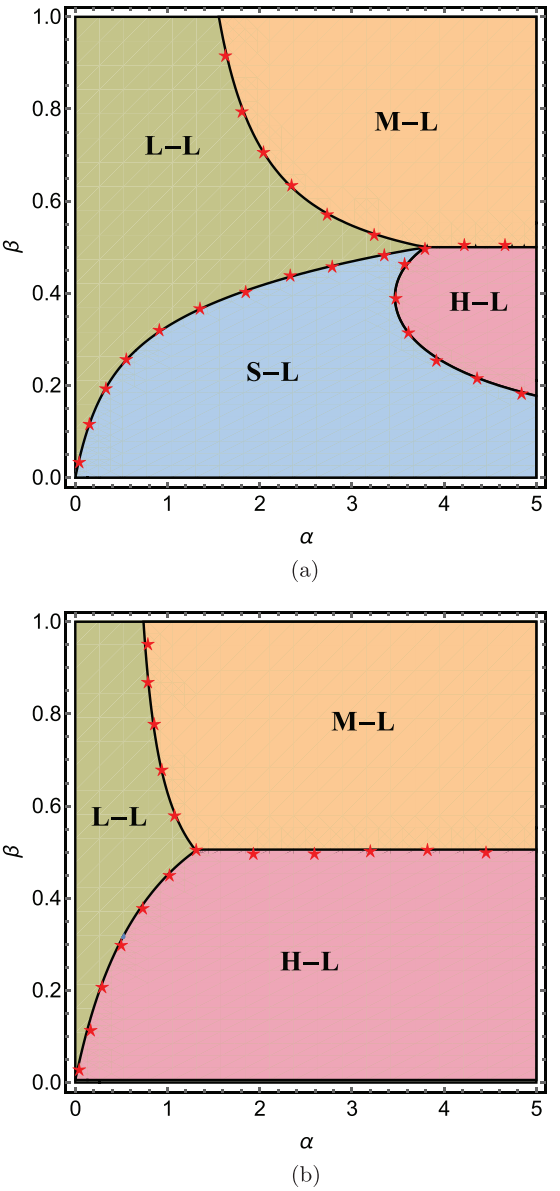

FIG. 8. Stationary phase diagrams for (a) $\mu_+ = 1$ and (b) $\mu_+ = 20$ with $\mu_- = 0.3$. Solid lines represent theoretical results and symbols correspond to Monte Carlo simulations. The length of the lattice is 1500.

of this phase requires $\alpha^+_{\text{eff}} > \beta$. It is compelling to mention that Fig. 9(b) corresponds to a circumstance where the system experiences the maximum number of phases at steady state. With further increasing μ_+, the M-L and H-L region expands followed by the shrinkage in L-L and S-L regions. Eventually, when $\mu_+ \to \infty$, the S-L phase disappears from the phase structure as shown in Fig. 9(b), with the system still displaying the other four stationary phases. In this case, initially, the number of phases displayed is 5, which reduces to 4, then further rises to 5, and finally decreases to 4.

Upon comparison of the phase diagram in the present case with that of the symmetric filling factor, the nature of the S-L phase is expected to have a distinct behavior. One can readily observe that the shock may move towards either of

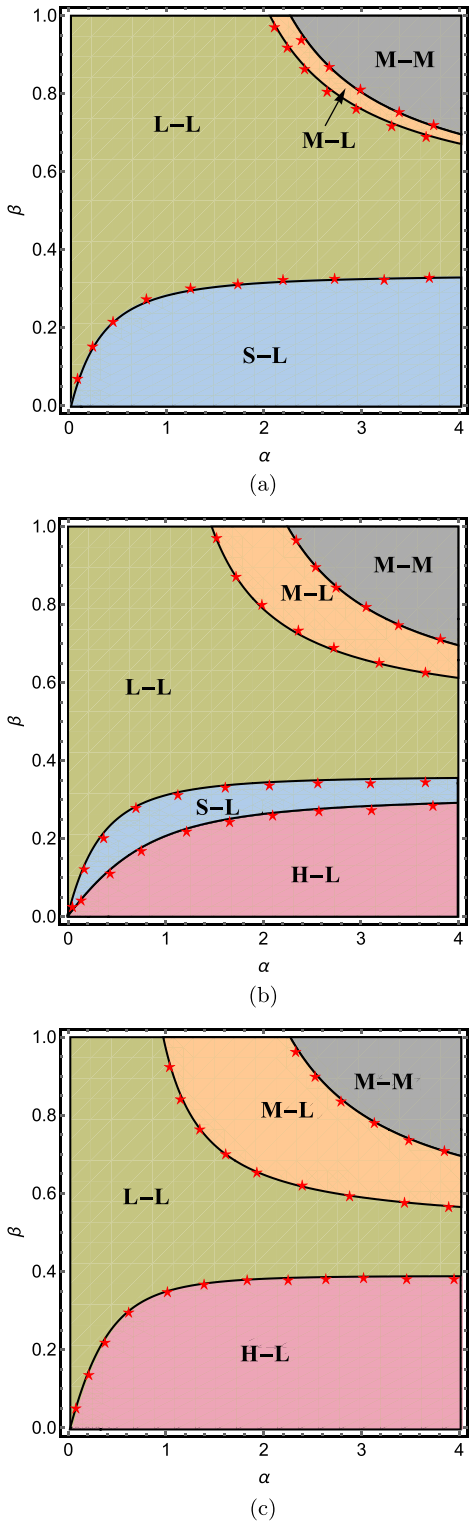

FIG. 9. Stationary phase diagrams for (a) $\mu_+ = 0.98$, (b) $\mu_+ = 1.5$, and (c) $\mu_+ = 15$ with $\mu_- = 0.9$. Solid lines represent theoretical results and symbols correspond to Monte Carlo simulations. The length of the lattice is set to 1500.

the boundaries with respect to β depending upon the fixed α [see Fig. 10(b)]. However, with respect to α, the shock moves towards the left for any constant value of β [see Fig. 10(c)]. The shock height has a behavior similar to the symmetric conditions and remains constant with the variation of α while other parameters are unchanged, whereas it decreases monotonically with respect to β, provided the remaining parameters are unaltered.

Finally, we intend to analyze how the filling factor μ_+ impacts the dynamics of the S-L phase for a fixed value of μ_-. Towards this direction, we have plotted Fig. 10(a), which depicts the variation of shock position and its change (inset) with respect to μ_+. Clearly, the shock enters from the right end and leaves the lattice from the left end with respect to μ_+ for $\mu_- = 0.3$. One can readily conclude that the variation is almost linear revealing that the shock position is nearly proportional to the filling factor of the concerning species.

2. *Stationary properties: Impact of μ_-*

Now, let us focus on the properties of the system for fixed μ_+ and varying values of μ_- such that $\mu_+ > \mu_-$. When $\mu_+ < 0.5$, two phases are realized in the phase diagram, namely L-L and S-L phases with the majority of the region covered by the L-L phase. One can see from Fig. 11(a) that, for $\mu_- < 0.5 < \mu_+ = 0.55$, four asymmetric phases are displayed by the system (L-L, M-L, S-L, and H-L). As μ_- takes the value 0.5, the H-L phase disappears from the phase diagram along with the shrinkage of S-L and M-L regions as shown in Fig. 11(b). This is because, with an increase in μ_-, enough negative particles are available in the system to hinder the movement of the positive particles. Mathematically, it is also affirmed by Eq. (B5) that the H-L phase does not persist for $\mu_- = 0.5$. As soon as $\mu_- > 0.5$, the maximal-maximal (M-M) phase emerges in the phase diagram changing its topology qualitatively [see Fig. 11(c)]. It is noteworthy to mention here that, when $\mu_+ > \mu_-$, the density of the positive particles always remains greater than that of the negative particles. One of the major consequences of coupling the system with two particle reservoirs having distinct filling factors is the appearance of the M-L phase in the phase diagram which has not been observed in previous studies [22,27]. For fixed α, β, and μ_+ chosen such that these parameters lie in the M-L region, we study the changes in the bulk densities for the two particle species. In this phase, the positive particles manifest maximal current phase with bulk density equal to 0.5, while the negative species depict an entrance dominated phase with the bulk density given by Eq. (B14). It can be noted that the value α_{eff}^- is entirely expressed in terms of α, β, and μ_-. As we plot the effective entrance rate α_{eff}^- against μ_- for $\alpha = 15$, $\beta = 0.8$, and $\mu_+ = 0.55$, it can be observed that α_{eff}^- increases with increase in μ_- [see Fig. 12(a)]. Eventually, at the critical point $\mu_- = 0.55$, α_{eff}^- takes the value 0.5, indicating the termination of low density phase corresponding to the $-$ particles. Now, to focus on the variation in particle density corresponding to negative species with respect to change in both α and β, we plotted ρ_- vs α for different values of β in Fig. 12(c). For fixed β, an increase in α enhances the inflow of negative species leading to an increase in the bulk density ρ_-. Similarly, upon varying the exit rate, the density corresponding to negative species increases with an increment in β [see Fig. 12(b)].

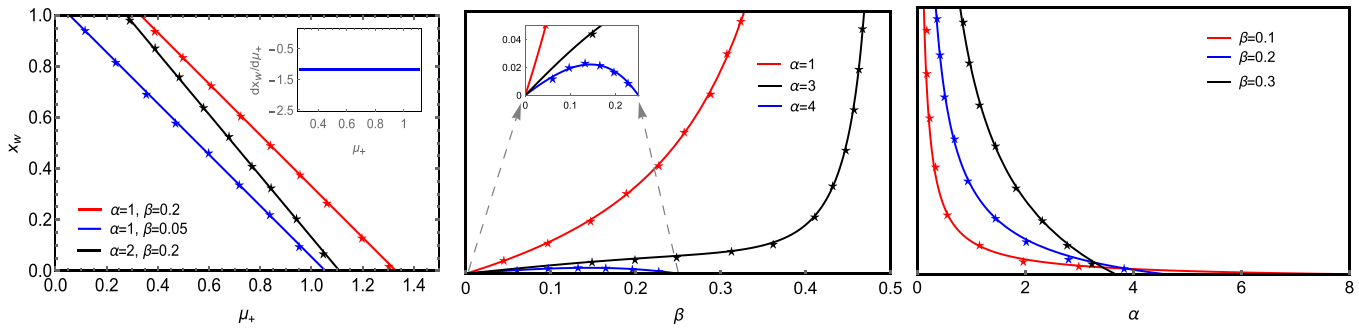

FIG. 10. Position of the shock vs (a) μ_+ with $\mu_- = 0.3$, (b) β with $\mu_+ = 1$, $\mu_- = 0.3$, and (c) α with $\mu_+ = 1$, $\mu_- = 0.3$. The rest of the parameter values are mentioned in the respective figures. Inset in (a) shows the change in x_w with respect to μ_+, which is almost linear. Inset in (b) is a zoomed figure for smaller values of β. In all figures, solid lines represent theoretical results and symbols correspond to Monte Carlo simulations. The length of the lattice is set to 1500.

Furthermore, it is necessary to point out the essential feature of the asymmetric M-M phase. Even though the bulk densities for both species in the M-M phase take the value 0.5, this phase is not identical to MC-MC, as in the former case the boundary densities corresponding to + and − particles are different. It is also evident from Eq. (B19) that, for $\mu_+ \neq \mu_-$,

$$\alpha^+_{\text{eff}} - \alpha^-_{\text{eff}} = \frac{\alpha\beta(\mu_+ - \mu_-)}{\prod_{j\in\{+,-\}}[2\beta\mu_j + \alpha(2\mu_j - 1)]} \neq 0. \quad (27)$$

In the above analysis, our discussion was focused on the case $\mu_+ \geqslant \mu_-$. The feasible phases, density profiles, and phase diagrams for the case when $\mu_+ < \mu_-$ can be obtained from the results acquired when $\mu_+ > \mu_-$ by the implementation of the following transformation:

$$\begin{aligned} \rho_+ &\leftrightarrow \rho_-, \\ \mu_+ &\leftrightarrow \mu_-, \\ \text{A-B phase} &\leftrightarrow \text{B-A phase}. \end{aligned} \quad (28)$$

We summarize eleven possible distinct regimes identified for different filling factors in Fig. 13. Without loss of generality, for the case when $\mu_+ = \mu_-$, we have assumed that the particle density of positive particles is greater than that of the negative species, i.e., the system displays H-L and S-L phases along the line $\mu_+ = \mu_-$. The density profiles corresponding to different phases are shown in Fig. 14.

V. SWAPPING RATE OF TWO SPECIES OTHER THAN 1 (s < 1)

Our above investigation, as well as previous studies [27,34], reveal that the predictions of the mean-field approximation are consistently supported by Monte Carlo simulations in the case of $s = 1$. Several attempts have been made focusing on the case when the exchange rate of the two particle species if they encounter each other is not equal to 1 [8,27]. It is reasonable to anticipate that the mean-field technique will also perform admirably for the case of $s \neq 1$ as well. In this direction, if the mean-field approximation is employed on Eqs. (4) and (5), we obtain the bulk currents corresponding to both the particle species as

$$\begin{aligned} J_+^{i-1,i} &= \rho_+^{i-1}(1 - \rho_+^i - \rho_-^i) + s\rho_+^{i-1}\rho_-^i, \\ J_-^{i+1,i} &= \rho_-^{i+1}(1 - \rho_-^i - \rho_+^i) + s\rho_-^{i+1}\rho_+^i. \end{aligned} \quad (29)$$

Applying a similar approach as discussed in Sec. II, we use Taylor's series expansion for $\rho_{i\pm1}$ and, retaining the terms up to second order, the continuum equation obtained using a mean-field approach given by Eq. (29) reduces to

$$\begin{aligned} \frac{\partial\rho_\pm}{\partial t} = \frac{\partial}{\partial x}\left(\frac{\epsilon}{2}\frac{\partial\rho_\pm}{\partial x} \mp \rho_\pm(1-\rho_\pm)\right) \\ \pm (1-s)\left(\rho_+\frac{\partial\rho_-}{\partial x} + \rho_-\frac{\partial\rho_+}{\partial x}\right) \\ \pm (1-s)\frac{\epsilon}{2}\left(\rho_+\frac{\partial^2\rho_-}{\partial x^2} - \rho_-\frac{\partial^2\rho_+}{\partial x^2}\right). \end{aligned} \quad (30)$$

This equation can be solved numerically by using a finite difference scheme, which has been outlined in Appendix C. It has been discovered that this solution highly depends upon the initial densities of the two species and does not match with the simulation results [see Fig. 15(a)], while, in some cases, agreement between simulations and mean-field results are remarkable [see Fig. 15(b)]. This depicts the failure of the mean-field theory in case the switching rate of the two particle species is not equal to 1. The identical observation was also made previously in Ref. [27] for the case of an infinite reservoir. Therefore, an alternate technique needs to be used to capture the system properties theoretically for $s \neq 1$, which will require further investigation.

VI. SUMMARY AND CONCLUSIONS

To summarize, we investigate a theoretical model that mimics the bidirectional movement of particles along a one-dimensional track, as is seen in the movement of cargo vesicles driven by motor proteins on microtubules and vehicular traffic on narrow roads. This model can be viewed as a two species bidirectional totally asymmetric simple exclusion process with distinct finite particle reservoirs for each species. The entry of each particle species on the lattice is governed

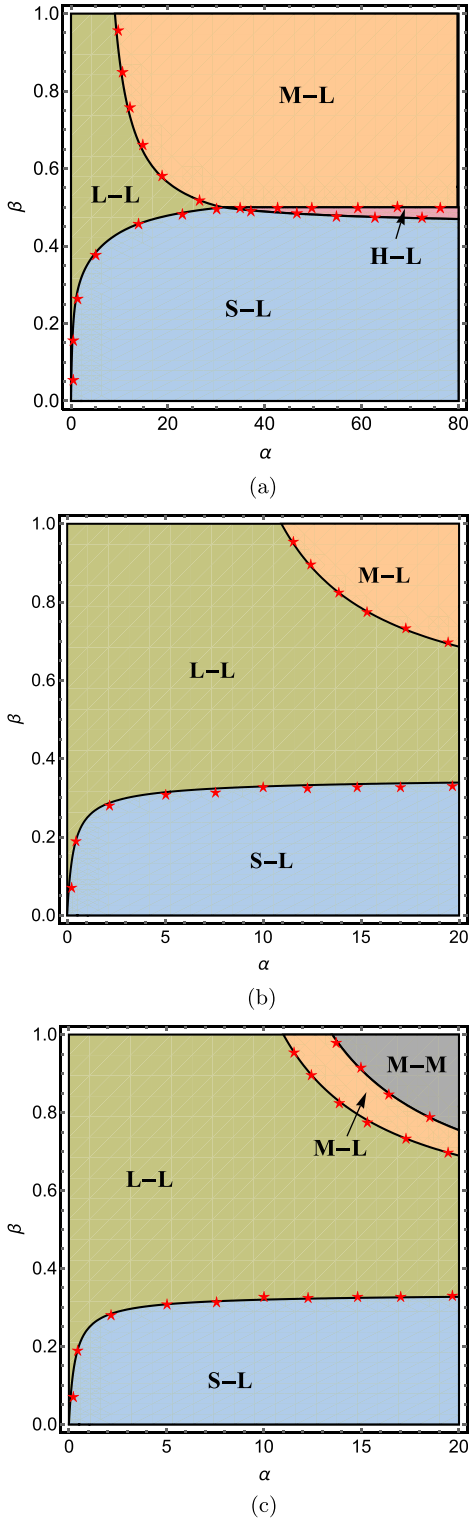

FIG. 11. Stationary phase diagrams for (a) $\mu_- = 0.3$, (b) $\mu_- = 0.5$, and (c) $\mu_- = 0.54$ with $\mu_+ = 0.55$. Solid lines represent theoretical results and symbols correspond to Monte Carlo simulations. The length of the lattice is taken to be 1500.

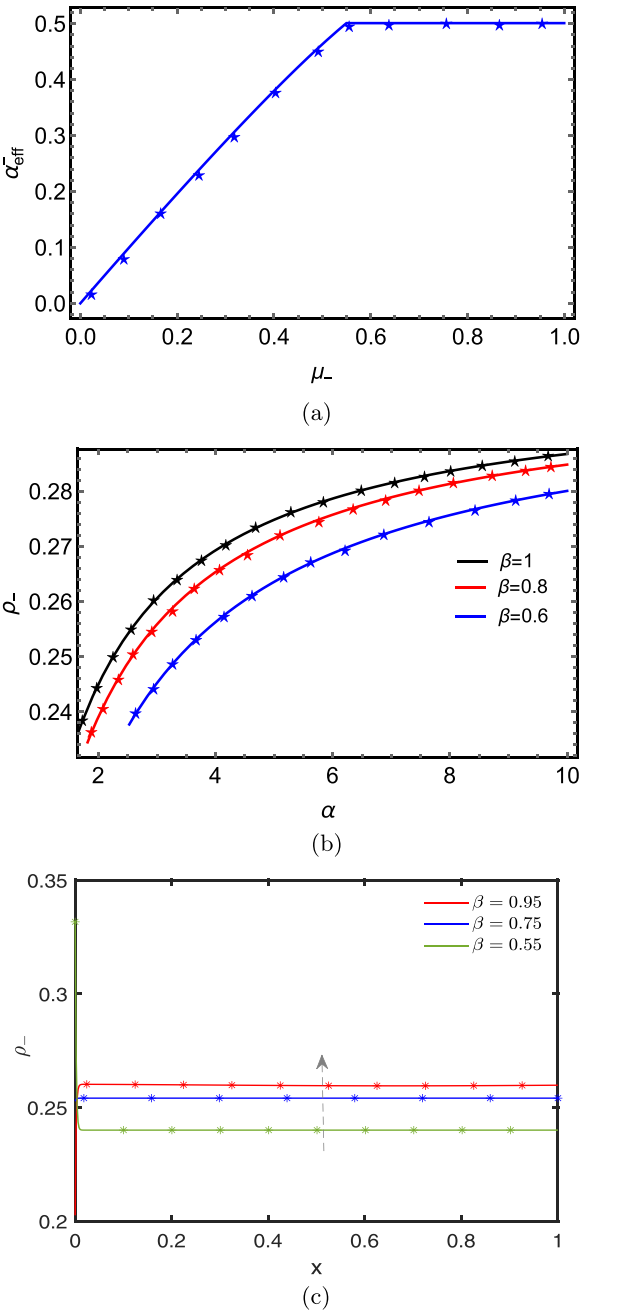

FIG. 12. (a) Effective entrance rate α^-_{eff} with respect to μ_- for $\mu_+ = 0.55$, $\alpha = 15$, and $\beta = 0.8$. (b) Particle density ρ_- with respect to α for distinct values of β. (c) Density profiles of the negative species for different values of β, $\alpha = 3$, $\mu_+ = 1$, and $\mu_- = 0.3$. The rest of the parameter values are mentioned in the respective figures. In all figures, solid lines represent theoretical results and symbols correspond to Monte Carlo simulations. The length of the lattice is taken to be 1500.

by the occupancy of the respective particle reservoir. The total number of particles for each species remains constant in the system and is characterized by the corresponding filling factor. Our model significantly differs from the previous studies where only one unified reservoir is taken into account. We theoretically examine the effect of the system dynamics on the crucial steady-state properties, such as phase diagrams, density profiles, phase boundaries, and phase transitions, in the framework of mean-field theory. All these theoretical outcomes are validated through extensive Monte Carlo simulations.

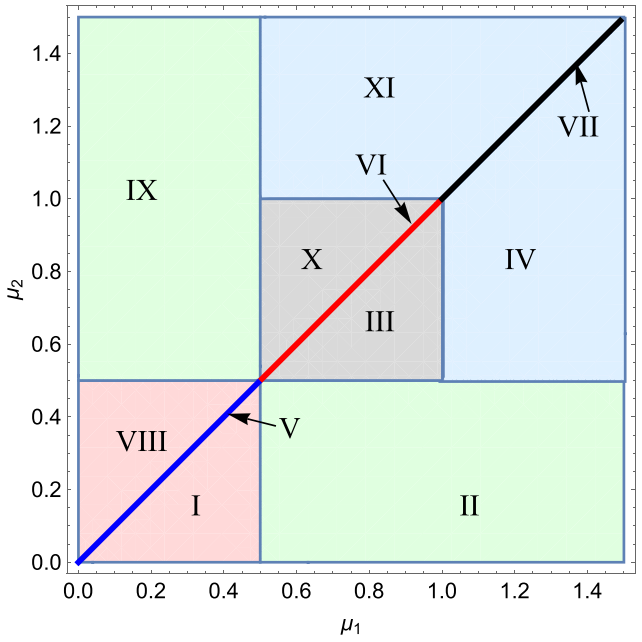

FIG. 13. Different dynamic regions based on the filling factors μ_+ and μ_-. Eleven distinct regions numbered I to XI have phase regimes that are qualitatively different. Table II provides a tabular description of the phase regimes that can exist in each of these different regions. In the table, a phase that does not exist is indicated by empty entries.

To study the impact of coupling the lattice to different finite reservoirs, we have explicitly considered two different scenarios: (i) the symmetric case when the filling factors for both the species are equal and (ii) the asymmetric case where these factors are different. In the former case, we observe a maximum of five stationary phases, two symmetric phases namely low density (LD-LD), maximal current phase (MC-MC), and three asymmetric phases: low-low density (L-L), shock-low density (S-L), and high-low density (H-L) phase. Despite the dynamics of the two species being identical, symmetry breakdown is recorded in this case, which persists even for a very small magnitude of the filling factor. Further, particle density histograms are studied to examine the effect of this phenomenon through Monte Carlo simulation results. The S-L phase is an asymmetric phase that has not been previously obtained in bidirectional systems with infinite resources. The number of perceived phases in the phase diagram changes from $3 \to 4 \to 5 \to 4$ with increasing values of the common filling factor, which represents a nonmonotonic trend.

TABLE II. The phases that exists in eleven different possible phase regions of the bidirectional system. The empty entries denote the phase that does not exist in the corresponding region.

Phase	I	II	III	IV	V	VI	VII	VIII	IX	X	XI
S-L	√	√	√	√	√	√	√				
H-L		√		√			√				
M-L		√	√	√							
MC-MC						√	√				
L-L	√	√	√	√	√	√	√	√	√	√	√
LD-LD					√	√		√			
M-M			√	√						√	√
L-M									√	√	√
L-H									√		√
L-S								√	√	√	√

For the case when the filling factors are unequal, a maximum of $4^2 = 16$ asymmetric phases can be observed in the system. Out of these, only eight phases are realized in the phase schema and the rest are discarded based on either physical or analytical arguments. Since, in this category, the two filling factors always remain different, the system cannot manifest a symmetric phase. The introduction of asymmetric filling factors leads to significant changes in the phase structure both quantitatively and qualitatively. A noteworthy feature of the phase diagrams is the presence of maximal-low (M-L) and maximal-maximal (M-M) phases which have not been detected in analogous systems with infinite resources. Even in this case, the variation in the number of phases in the phase diagram shows a nonmonotonic trend.

For deeper analysis of the S-L phase, we study the position and the height of the shock as well as the particle densities of both the species with respect to change in all the parameters: entry-exit rates and the filling factors. The exact number, dynamic characteristics, and region of various phases rely on the number of particles in each reservoir. We have identified the critical points where the appearance and disappearance of phases occur in the system.

It is important to note that the proposed model differs from the previous study [32] in several ways. Unlike the bidirectional system with reservoir crowding and a global constraint on the total number of particles in the system examined in the previous study, the current model imposes a global constraint on the number of resources of an individual species and regulates only the entrance rates based on the reservoir's capacity. Additionally, the present model introduces another feature—the M-L phase, which was not observed in Ref. [32]. All the phase boundaries in the present study exhibit a concave downward shape, in contrast to the convex upward trend, observed in the case of a unified reservoir [32].

The proposed model is an attempt to qualitatively understand the steady-state properties of a bidirectional system with a constraint on the number of particles of both species. This study might contribute to a greater understanding of the intricate dynamics in numerous biological and physical transport processes, both natural and man-made. It is significant to mention here that the study of our model in the case of $s \neq 1$ may be rather convoluted and it is difficult to conclude anything from the proposed analysis which works very well for $s = 1$. This situation may be addressed in our subsequent works. Additionally, the model can be generalized by including dynamics such as the creation and annihilation of particles on the lattice, which might add intriguing features to the system's stationary properties.

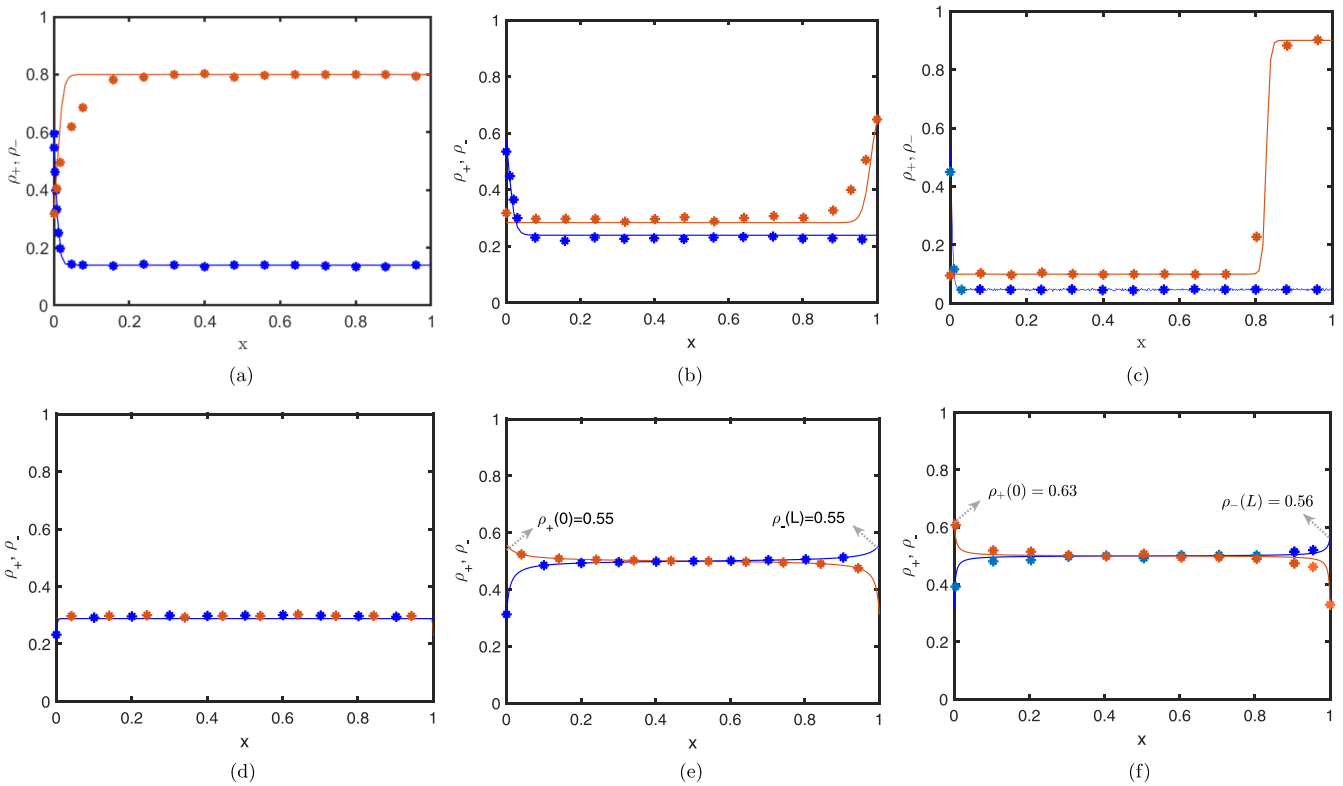

FIG. 14. Density profiles for (a) H-L, (b) L-L, (c) S-L phases, (d) LD-LD and (e) MC-MC with $(\alpha, \beta, \mu) = (2, 0.2, 10)$, $(2, 0.315, 1.1)$, $(1, 0.1, 0.3)$, $(1, 0.5, 0.9)$, and $(3.5, 0.8, 1.1)$ with symmetric filling factors, and (f) M-M phase with $(\alpha, \beta, \mu_+, \mu_-) = (4.5, 0.8, 15, 0.9)$. The lattice length is taken to be 1500. Red and blue solid lines are mean-field results for + and − particles, respectively, while filled markers correspond to Monte Carlo simulations.

ACKNOWLEDGMENTS

A.G. thanks the Council of Scientific and Industrial Research (CSIR), India for financial support under File No. 09/1005(0023)/2018-EMR-I. A.K.G. acknowledges support from DST-SERB, Government of India (Grants No. CRG/2019/004669 and No. MTR/2019/000312). This work was partially supported by the FIST program of the Department of Science and Technology, Government of India, Ref. No. SR/FST/MS-I/2018/22(C).

APPENDIX A: SYMMETRIC PHASES

There are two feasible symmetric phases for which the explicit expressions for the phase boundaries, particle density, and the effective entrance rate α_{eff} can be theoretically computed by utilizing the framework presented in Secs. II and III A. In all of these phases, the two species of particles display identical stationary properties, which are examined in the following discussion.

(i) Low density phase (LD-LD). In this phase, both the species of the particles are in low density with bulk densities equal to α_{eff} and the current corresponding to both the particle species is equal to

$$J_+ = J_- = \alpha_{\text{eff}}(1 - \alpha_{\text{eff}}). \tag{A1}$$

As a result, Eq. (20) reduces to

$$\mu = \rho_r + \alpha_{\text{eff}}. \tag{A2}$$

Upon solving Eqs. (21) and (A2) along with the fact that $\alpha^+_{\text{eff}} = \alpha^-_{\text{eff}}$, the reservoir quotient is obtained as

$$\rho_r = \frac{1}{2\alpha}(\alpha(\mu - \beta) - \beta\mu + \sqrt{4\alpha\beta\mu^2 + [\alpha(\mu - \beta) - \beta\mu]^2}). \tag{A3}$$

The existential conditions of this phase require the effective entrance to be less than 0.5 and β, which leads to

$$\min\{0.5,\ \beta\} > \frac{1}{2\alpha}(\alpha(\mu + \beta) + \beta\mu - \sqrt{4\alpha\beta\mu^2 + [\alpha(\mu - \beta) - \beta\mu]^2}). \tag{A4}$$

Note that, in the limiting case of $\mu \to \infty$, α_{eff} is given by $\alpha\beta/(\alpha + \beta)$, which matches with the corresponding effective entry rate obtained for the LD-LD phase in the case of the bidirectional model with no restriction on the number of particles in the system [27].

(ii) Maximal current phase (MC-MC). This case persists when both the particle species are individually in the MC phase with bulk densities 0.5 and bulk particle currents $J_+ = J_- = 0.25$. Such a phase is characterized by the following conditions:

$$\alpha_{\text{eff}} > 0.5, \quad \beta > 0.5. \tag{A5}$$

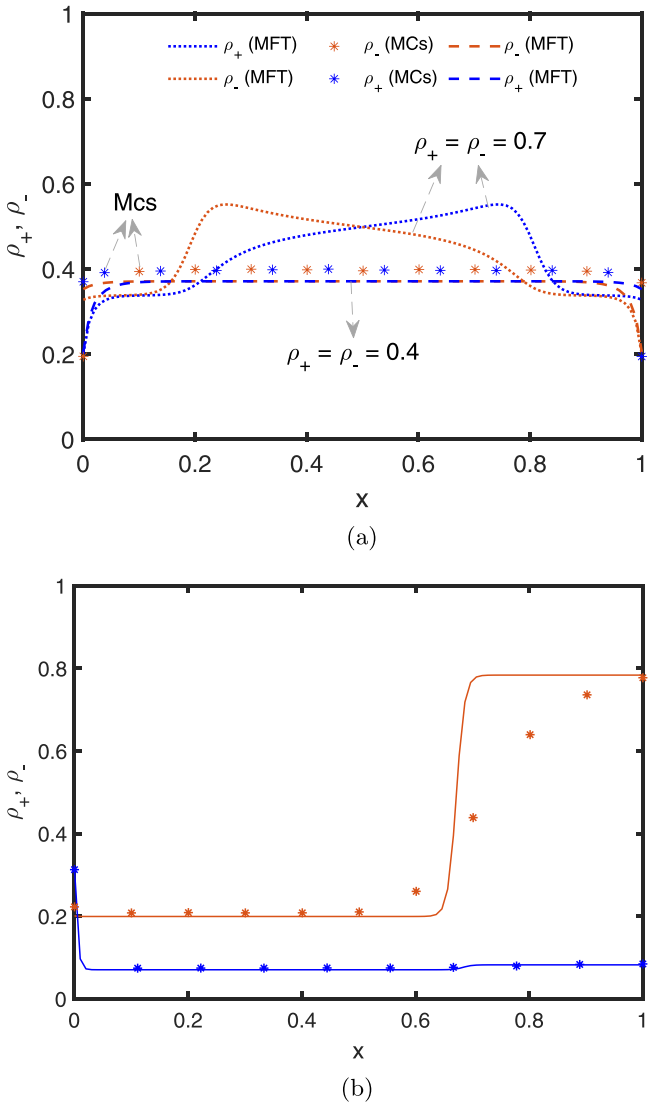

FIG. 15. (a) Density profile of the two particle species for $\alpha = 0.7$, $\beta = 1$, $\mu_1 = \mu_2 = 1.1$, and $s = 0.8$ obtained using mean-field theory. Dashed lines correspond to solution obtained with initial condition $\rho_+ = \rho_- = 0.4$, dotted line is plotted for initial condition $\rho_+ = \rho_- = 0.7$, and symbols correspond to Monte Carlo simulations. (b) Density profile of the two particle species for $\alpha = 0.5$, $\beta = 0.2$, $\mu_1 = \mu_2 = 1.1$, and $s = 0.8$. Solid lines represent mean-field results and symbols correspond to Monte Carlo simulations.

Using Eq. (20), we have

$$\rho_r = \mu - 0.5, \tag{A6}$$

which provides the existential conditions in the $\alpha - \beta$ plane as

$$\alpha > \frac{2\beta\mu}{(2\mu-1)(2\beta-1)}, \quad \beta > 0.5. \tag{A7}$$

Further, it is evident from Eq. (A6) that the MC-MC phase exists only when

$$\mu > 0.5. \tag{A8}$$

For $\mu \to \infty$, Eq. (A7) reduces to $\alpha > \frac{\beta}{2\beta-1}$, which is the condition for the MC-MC phase in the standard bidirectional TASEP with a common reservoir containing infinite resources [27].

APPENDIX B: ASYMMETRIC PHASES

In each of the asymmetric phases discussed below, first the effective entrance rates $\alpha_{\rm eff}^+$ and $\alpha_{\rm eff}^-$ are computed, which are then utilized to determine particle densities, the position of shock, and existential criteria in each phase.

(i) High-low density phase (H-L). It is assumed that the + particles exhibit high density phase where density is greater than 0.5 and the − particles portray low density phase. Employing the expressions for currents given by Eq. (15), we attain

$$J_+ = \beta(1-\beta), \quad J_- = \alpha_{\rm eff}^-(1-\alpha_{\rm eff}^-). \tag{B1}$$

Substituting the above expressions of J_+ and J_- in Eq. (18), the value of effective entrance rates is procured as

$$\alpha_{\rm eff}^- = \frac{1}{2\mu_-}\left(\alpha\rho_{r_-} + \mu_- - \sqrt{(\alpha\rho_{r_-}+\mu_-)^2 - 4\alpha\beta\mu_-\rho_{r_-}}\right),$$
$$\alpha_{\rm eff}^+ = \frac{\alpha(\beta-1)\beta^2\rho_{r_+}}{\alpha\rho_{r_+}(\alpha_{\rm eff}^- - 1)\alpha_{\rm eff}^- + \beta^2\mu_+(\beta-1)}. \tag{B2}$$

Utilizing the particle number conservation given by Eq. (20) provides

$$\mu_+ = \rho_{r_+} + 1 - \beta, \quad \mu_- = \rho_{r_-} + \alpha_{\rm eff}^-, \tag{B3}$$

which along with Eq. (B2) gives the reservoir quotients as

$$\rho_{r_+} = \mu_+ - (1-\beta),$$
$$\rho_{r_-} = \frac{\left(\alpha(\mu_- - \beta) + \mu_-(2\mu_- - 1) + \left\{\alpha(\mu_- - \beta)\right.\right.}{2(\alpha+\mu_-)}$$
$$+ \frac{\left.\left.\mu_-(2\mu_- - 1)^2 + 4(1-\mu_-)\mu_-^2(\alpha+\mu_-)\right\}^{0.5}\right)}{2(\alpha+\mu_-)}. \tag{B4}$$

These calculated values of the reservoir quotients can be replaced in Eq. (B2) to obtain the effective entrance rates. The feasible region corresponding to this phase satisfies

$$\beta < \min\{\alpha_{\rm eff}^+, 0.5\}, \quad \alpha_{\rm eff}^- < \min\{\beta, 0.5\}, \tag{B5}$$

along with the filling factors satisfying $\mu_+ \geqslant \mu_-$ and $\mu_+ > 0.5$. Moreover, the condition $\alpha_{\rm eff}^+ > \beta$ is satisfied only if $\mu_- < 0.5 < \mu_+$ or $(0.5 < \mu_-$ and $1 < \mu_+)$. It is worth pointing out that, in case both the filling factors are equal, the SSB phenomenon is observed. Moreover, all the stationary properties such as particle densities, reservoir's quotients, and the particle currents for the case of symmetric filling factors can be calculated by substituting $\mu_+ = \mu_- = \mu$ in all the above obtained expressions.

Clearly, when both $\mu_+ \to \infty$ and $\mu_- \to \infty$, the conditions for the existence of the H-L phase in a bidirectional system with an infinite particle reservoir is recovered [27].

(ii) Shock-low density phase (S-L). We presume that the + particles display shock phase, while the − particles are in

low density phase. This phase persists when the boundary-controlling parameters assure the following constraints:

$$\begin{aligned} J_+ &= \beta(1-\beta) = \alpha^+_{\text{eff}}(1-\alpha^+_{\text{eff}}),\\ J_- &= \alpha^-_{\text{eff}}(1-\alpha^-_{\text{eff}}),\\ \int_0^1 \rho_+\, dx &= \int_0^{x_w} \alpha^+_{\text{eff}}\, dx + \int_{x_w}^1 (1-\beta)\, dx, \end{aligned} \tag{B6}$$

where x_w is the position of shock in the density profile. The effective entrance rates for the particles can be retrieved from Eq. (18) as

$$\begin{aligned} \alpha^-_{\text{eff}} &= \frac{1}{2\mu_-}(\mu_- + \alpha\rho_{r_-} - \sqrt{(\mu_- + \alpha\rho_{r_-})^2 - 4\alpha\beta\mu_-\rho_{r_-}}),\\ \alpha^+_{\text{eff}} &= \frac{1}{2\beta\mu_+}(\beta\mu_+ + \alpha\beta\rho_{r_+} - \{\beta[\beta(\mu_+ - \alpha\rho_{r_+})^2\\ &\quad - 4\alpha(\alpha^-_{\text{eff}} - 1)\alpha^-_{\text{eff}}\mu_+\rho_{r_+}]\}^{0.5}). \end{aligned} \tag{B7}$$

Now we make use of Eq. (20) to calculate the reservoir quotient for $-$ particles, which yields

$$\begin{aligned} \rho_{r_-} &= \frac{1}{2(\alpha+\mu_-)}(\alpha(\mu_- - \beta) + \mu_-(2\mu_- - 1)\\ &\quad + \sqrt{\alpha^2(\beta-\mu_-)^2 + \mu_-^2 + 2\alpha\mu_-[\beta + \mu_-(1-2\beta)]}). \end{aligned} \tag{B8}$$

Since the existence of such a phase requires $\alpha^+_{\text{eff}} = \beta$, we have

$$\rho_{r_+} = \frac{(\beta-1)\beta^2\mu_+}{\alpha[\alpha^-_{\text{eff}}(1-\alpha^-_{\text{eff}}) + \beta(\beta-1)]}. \tag{B9}$$

The position of the shock can be procured by utilizing Eqs. (20) and (B6) along with Eqs. (B8) and (B10), as

$$x_w = \frac{\beta + \mu_+ - \rho_{r_+} - 1}{2\beta - 1}. \tag{B10}$$

Finally, the boundary parameters must satisfy the following conditions for the S-L phase to exist:

$$0 \leqslant x_w \leqslant 1, \quad \alpha^-_{\text{eff}} < \min\{\beta, 0.5\}. \tag{B11}$$

It must be noted that, when $\mu_+ = \mu_-$, spontaneous symmetry breaking is observed in the system and the corresponding results can be attained by replacing μ_+ and μ_- by μ in all the above expressions. Furthermore, this phase vanishes when both μ_+ and μ_- tend to ∞.

(iii) Maximal-low phase (M-L). In this phase, it is assumed that the $+$ particles manifest maximal current with density given by 0.5, whereas the average particle density of $-$ particles remains less than 0.5. Here, the particle currents are

$$J_+ = 0.25, \quad J_- = \alpha^-_{\text{eff}}(1-\alpha^-_{\text{eff}}). \tag{B12}$$

These expressions when substituted in Eq. (18) and solved for the effective entrance rates provide

$$\begin{aligned} \alpha^-_{\text{eff}} &= \frac{1}{2\beta\mu_-}(\beta(\mu_- + \alpha\rho_{r_-})\\ &\quad - \sqrt{\beta[\alpha\mu_-\rho_{r_-} + \beta(\mu_- - \alpha\rho_{r_-})^2]}),\\ \alpha^+_{\text{eff}} &= \frac{\beta\alpha\rho_{r_+}}{\beta\mu_+ + 4\alpha\rho_{r_+}J_-}, \end{aligned} \tag{B13}$$

and further α^+_{eff} can be calculated. Moreover, from Eqs. (20) and (B14), we have

$$\rho_{r_+} = \mu_+ - 0.5, \tag{B14}$$

$$\begin{aligned} \rho_{r_-} &= \frac{(\alpha[4\beta(\mu_- - 1) + 1] + 4\beta\mu_-(2\mu_- - 1)}{8\beta(\alpha + \mu_-)}\\ &\quad + \{(\alpha[1 + 4\beta(\mu_- - 1)] + 4\mu_-\beta(2\mu_- - 1))^2\\ &\quad - 64\beta^2(\mu_- - 1)\mu_-^2(\mu_- + \alpha)\}^{0.5}). \end{aligned} \tag{B15}$$

Using the above obtained expressions for the boundary parameters, the conditions of existence for this phase are framed as

$$\begin{aligned} &\min\{\alpha^+_{\text{eff}}, \beta\} > 0.5 > \alpha^-_{\text{eff}},\\ &\mu_+ > \max\{\mu_-, 0.5\}. \end{aligned} \tag{B16}$$

(iv) Maximal-maximal phase (M-M). All the stationary properties of this phase are similar to the MC-MC phase except the fact that here $\alpha^+_{\text{eff}} \neq \alpha^-_{\text{eff}}$, which further implies $\mu_+ \neq \mu_-$. In this phase, the reservoirs' quotients are given by $\rho_{r_j} = \mu_j - 0.5$ for $j \in \{+, -\}$. Since these quotients must be non-negative, the existential criteria for this phase are

$$\min\{\mu_+, \mu_-\} > 0.5, \quad \min\{\alpha^+_{\text{eff}}, \alpha^-_{\text{eff}}, \beta\} > 0.5, \tag{B17}$$

where

$$\alpha^+_{\text{eff}} = \frac{\alpha\rho_{r_+}}{\beta\mu_+ + \alpha\rho_{r_+}}, \quad \alpha^-_{\text{eff}} = \frac{\alpha\rho_{r_-}}{\beta\mu_- + \alpha\rho_{r_-}}. \tag{B18}$$

(v) Low-low density phase (L-L). This phase exists when the particle densities for both species are entry dominated and remain less than 0.5. Such a phase exists when

$$\alpha^+_{\text{eff}} < \min\{\beta, 0.5\}, \quad \alpha^-_{\text{eff}} < \min\{\beta, 0.5\}. \tag{B19}$$

The corresponding particle currents are expressed as

$$J_+ = \alpha^+_{\text{eff}}(1-\alpha^+_{\text{eff}}), \quad J_- = \alpha^-_{\text{eff}}(1-\alpha^-_{\text{eff}}). \tag{B20}$$

Utilizing the fact that the particles are conserved along with $\rho_+ = \alpha^+_{\text{eff}}$ and $\rho_- = \alpha^-_{\text{eff}}$, we have

$$\rho_{r_+} = \mu_+ - \alpha^+_{\text{eff}}, \quad \rho_{r_-} = \mu_- - \alpha^-_{\text{eff}}. \tag{B21}$$

Solving Eq. (18) along with Eqs. (B20) and (B21), the effective entrance rates for both species can be obtained. In the case of symmetric filling factors, one can substitute $\mu_+ = \mu_- = \mu$ in all of the above expressions.

The existential conditions of the phases such as L-S, L-M, and L-H can be obtained by interchanging the roles of the parameters for the $+$ and the $-$ particles in S-L, M-L, and H-L phases, respectively.

APPENDIX C: NUMERICAL SCHEME

In this section, we delineate a numerical approach to obtain the density profiles for the bidirectional system. Our system seems quite simple but it is difficult to solve second order differential equations (13) and (30) analytically. The term involving time is retained in the system and steady-state particle density for both the species is captured in the limit $t \to \infty$, where t is the total number of time steps to guarantee the

occurrence of steady state. The differential equation is discretized by choosing $\Delta x = 1/L$ and Δt is selected so that the stability criteria $\Delta t/\Delta x^2 \leqslant 1$ is maintained. Time and the space derivatives involved in the equation are replaced with forward and central difference formulas. Denoting the approximation to ρ_j at $(i\Delta x, n\Delta t)$ by $\rho_j^{i,n}$ for $j \in \{+, -\}$, we obtain the following equations:

$$\begin{aligned}\rho_+^{i,n+1} &= \rho_+^{i,n} + \frac{\epsilon\Delta t}{2}(1-s)\rho_+^{i,n}\left(\frac{\rho_-^{i+1,n} - 2\rho_-^{i,n} + \rho_-^{i-1,n}}{\Delta x^2}\right) \\ &+ \frac{\epsilon\Delta t}{2}[1-(1-s)\rho_-^{i,n}]\left(\frac{\rho_+^{i+1,n} - 2\rho_+^{i,n} + \rho_+^{i-1,n}}{\Delta x^2}\right) \\ &+ \Delta t[2\rho_+^{i,n} - 1 + (1-s)\rho_-^{i,n}]\left(\frac{\rho_+^{i+1,n} - \rho_+^{i-1,n}}{2\Delta x}\right) \\ &+ \Delta t\ (1-s)\rho_-^{i,n}\left(\frac{\rho_-^{i+1,n} - \rho_-^{i-1,n}}{2\Delta x}\right) \qquad \text{(C1)}\end{aligned}$$

for the positive particles. Since the above equation is not valid for $i = 1$ and $i = L$ and both the species interact explicitly only at the boundaries, we cannot directly include boundary conditions in the above discretization. Instead, we utilize Eqs. (7) and (8), which can be written as

$$\begin{aligned}\rho_+^{1,n+1} &= \rho_+^{1,n} + \Delta t\left[\alpha\left(1 - \frac{\sum \rho_+^{i,n}}{L\mu_+}\right)(1 - \rho_+^{1,n} - \rho_-^{1,n})\right. \\ &\left. - \rho_+^{1,n}(1 - \rho_+^{2,n} - \rho_-^{2,n}) - s\rho_+^{1,n}\rho_-^{2,n}\right], \\ \rho_+^{L,n+1} &= \rho_+^{L,n} + \Delta t[\rho_+^{L-1,n}(1 - \rho_+^{L,n} - \rho_-^{L,n}) \\ &+ s\rho_+^{L-1,n}\rho_-^{L,n} - \beta\rho_+^{L,n}]. \qquad \text{(C2)}\end{aligned}$$

In the case of $s = 1$, Eq. (C1) simplifies considerably and is given by

$$\begin{aligned}\rho_+^{i,n+1} &= \rho_+^{i,n} + \frac{\epsilon\Delta t}{2}\left(\frac{\rho_+^{i+1,n} - 2\rho_+^{i,n} + \rho_+^{i-1,n}}{\Delta x^2}\right) \\ &+ \Delta t\left(\frac{\rho_+^{i+1,n} - \rho_+^{i-1,n}}{2\Delta x}\right)(2\rho_+^{i,n} - 1). \qquad \text{(C3)}\end{aligned}$$

Similar equations can be written for the negative particles as well.

[1] B. Alberts, A. Johnson, P. Walter, J. Lewis, M. Raff, and K. Roberts, *Molecular Cell Biology* (Garland Science, New York, 2008).

[2] C. Appert-Rolland, M. Ebbinghaus, and L. Santen, Intracellular transport driven by cytoskeletal motors: General mechanisms and defects, Phys. Rep. **593**, 1 (2015).

[3] D. Chowdhury, L. Santen, and A. Schadschneider, Statistical physics of vehicular traffic and some related systems, Phys. Rep. **329**, 199 (2000).

[4] M. Schreckenberg, A. Schadschneider, K. Nagel, and N. Ito, Discrete stochastic models for traffic flow, Phys. Rev. E **51**, 2939 (1995).

[5] R. Mahnke, J. Kaupužs, and I. Lubashevsky, Probabilistic description of traffic flow, Phys. Rep. **408**, 1 (2005).

[6] V. Belitsky, J. Krug, E. J. Neves, and G. M. Schütz, A cellular automaton model for two-lane traffic, J. Stat. Phys. **103**, 945 (2001).

[7] B. Widom, J. L. Viovy, and A. D. Defontaines, Repton model of gel electrophoresis and diffusion, J. Phys. I (France) **1**, 1759 (1991).

[8] T. Chou and D. Lohse, Entropy-Driven Pumping in Zeolites and Biological Channels, Phys. Rev. Lett. **82**, 3552 (1999).

[9] V. Popkov and G. M. Schütz, Steady-state selection in driven diffusive systems with open boundaries, Europhys. Lett. **48**, 257 (1999).

[10] J. Krug, Boundary-Induced Phase Transitions in Driven Diffusive Systems, Phys. Rev. Lett. **67**, 1882 (1991).

[11] A. B. Kolomeisky, G. M. Schütz, E. B. Kolomeisky, and J. P. Straley, Phase diagram of one-dimensional driven lattice gases with open boundaries, J. Phys. A: Math. Gen. **31**, 6911 (1998).

[12] H. J. Hilhorst and C. Appert-Rolland, A multi-lane tasep model for crossing pedestrian traffic flows, J. Stat. Mech. (2012) P06009.

[13] B. Holldobler and E. O. Wilson, *The Ants* (Harvard University Press, Cambridge, MA, 1990).

[14] D. Chowdhury, A. Schadschneider, and K. Nishinari, Physics of transport and traffic phenomena in biology: From molecular motors and cells to organisms, Phys. Life Rev. **2**, 318 (2005).

[15] T. Chou and G. Lakatos, Clustered Bottlenecks in mRNA Translation and Protein Synthesis, Phys. Rev. Lett. **93**, 198101 (2004).

[16] C. T. MacDonald, J. H. Gibbs, and A. C. Pipkin, Kinetics of biopolymerization on nucleic acid templates, Biomol.: Original Res. Biomol. **6**, 1 (1968).

[17] C. T. MacDonald and J. H. Gibbs, Concerning the kinetics of polypeptide synthesis on polyribosomes, Biomol.: Original Res. Biom. **7**, 707 (1969).

[18] B. Derrida, E. Domany, and D. Mukamel, An exact solution of a one-dimensional asymmetric exclusion model with open boundaries, J. Stat. Phys. **69**, 667 (1992).

[19] B. Derrida, M. R. Evans, V. Hakim, and V. Pasquier, Exact solution of a 1d asymmetric exclusion model using a matrix formulation, J. Phys. A: Math. Gen. **26**, 1493 (1993).

[20] B. Derrida and M. R. Evans, The asymmetric exclusion model: exact results through a matrix approach, in *Non Equilibrium Statistical Mechanics in One Dimension*, edited by V. Privman (Cambridge University Press, Cambridge, UK, 1997), pp. 277–304.

[21] G. Schötz and E. Domany, Phase transitions in an exactly soluble one-dimensional exclusion process, J. Stat. Phys. **72**, 277 (1993).

[22] M. R. Evans, D. P. Foster, C. Godrèche, and D. Mukamel, Spontaneous Symmetry Breaking in a One Dimensional Driven Diffusive System, Phys. Rev. Lett. **74**, 208 (1995).

[23] V. Soppina, A. K. Rai, A. J. Ramaiya, P. Barak, and R. Mallik, Tug-of-war between dissimilar teams of microtubule motors regulates transport and fission of endosomes, Proc. Natl. Acad. Sci. USA **106**, 19381 (2009).

[24] W. O. Hancock, Bidirectional cargo transport: Moving beyond tug of war, Nat. Rev. Mol. Cell Biol. **15**, 615 (2014).

[25] T. Kretz, A. Grünebohm, M. Kaufman, F. Mazur, and M. Schreckenberg, Experimental study of pedestrian counterflow in a corridor, J. Stat. Mech. (2006) P10001.

[26] W. H. K. Lam, J. Lee, and C. Y. Cheung, A study of the bi-directional pedestrian flow characteristics at hong kong signalized crosswalk facilities, Transportation **29**, 169 (2002).

[27] M. R. Evans, D. P. Foster, C. Godrèche, and D. Mukamel, Asymmetric exclusion model with two species: Spontaneous symmetry breaking, J. Stat. Phys. **80**, 69 (1995).

[28] A. Jindal and A. K. Gupta, Exclusion process on two intersecting lanes with constrained resources: Symmetry breaking and shock dynamics, Phys. Rev. E **104**, 014138 (2021).

[29] N. Sharma and A. K. Gupta, Phase segregation and spontaneous symmetry breaking in a bidirectional two-channel non-conserving model with narrow entrances, J. Stat. Mech. (2017) 043211.

[30] M. Clincy, M. R. Evans, and D. Mukamel, Symmetry breaking through a sequence of transitions in a driven diffusive system, J. Phys. A: Math. Gen. **34**, 9923 (2001).

[31] V. Popkov and I. Peschel, Symmetry breaking and phase coexistence in a driven diffusive two-channel system, Phys. Rev. E **64**, 026126 (2001).

[32] B. Pal and A. K. Gupta, Persistence of spontaneous symmetry breaking in bidirectional transport system with reservoir crowding, J. Phys. A: Math. Theor. **54**, 405002 (2021).

[33] D. W. Erickson, G. Pruessner, B. Schmittmann, and R. K. P. Zia, Spurious phase in a model for traffic on a bridge, J. Phys. A: Math. Gen. **38**, L659 (2005).

[34] P. F. Arndt, T. Heinzel, and V. Rittenberg, First-order phase transitions in one-dimensional steady states, J. Stat. Phys. **90**, 783 (1998).

[35] A. K. Verma, N. Sharma, and A. K. Gupta, Far-from-equilibrium bidirectional transport system with constrained entrances competing for pool of limited resources, Phys. Rev. E **97**, 022105 (2018).

[36] A. Jindal, A. B. Kolomeisky, and A. K. Gupta, Effect of local dissociations in bidirectional transport of driven particles, J. Stat. Mech. (2020) 113202.

[37] A. Jindal and A. K. Gupta, Effect of local dissociation on symmetry breaking in exclusion model constituted by bridge lane and input-output taseps, Chaos Solitons Fractals **152**, 111354 (2021).

[38] L. J. Cook and R. K. P. Zia, Feedback and fluctuations in a totally asymmetric simple exclusion process with finite resources, J. Stat. Mech. (2009) P02012.

[39] L. J. Cook, R. K. P. Zia, and B. Schmittmann, Competition between multiple totally asymmetric simple exclusion processes for a finite pool of resources, Phys. Rev. E **80**, 031142 (2009).

[40] L. J. Cook, J. J. Dong, and A. LaFleur, Interplay between finite resources and a local defect in an asymmetric simple exclusion process, Phys. Rev. E **88**, 042127 (2013).

[41] C. A. Brackley, L. Ciandrini, and M. C. Romano, Multiple phase transitions in a system of exclusion processes with limited reservoirs of particles and fuel carriers, J. Stat. Mech. (2012) P03002.

[42] D. A. Adams, B. Schmittmann, and R. K. P. Zia, Far-from-equilibrium transport with constrained resources, J. Stat. Mech. (2008) P06009.

[43] A. K. Verma and A. K. Gupta, Stochastic transport on flexible lattice under limited resources, J. Stat. Mech. (2019) 103210.

[44] L. Ciandrini, I. Neri, J. C. Walter, O. Dauloudet, and A. Parmeggiani, Motor protein traffic regulation by supply-demand balance of resources, Phys. Biol. **11**, 056006 (2014).

[45] P. Greulich, L. Ciandrini, R. J. Allen, and M. C. Romano, Mixed population of competing totally asymmetric simple exclusion processes with a shared reservoir of particles, Phys. Rev. E **85**, 011142 (2012).

[46] A. Schadschneider, D. Chowdhury, and K. Nishinari, *Stochastic Transport in Complex Systems: From Molecules to Vehicles* (Elsevier, Amsterdam, 2010).

[47] J. Krug, Phase separation in disordered exclusion models, Braz. J. Phys. **30**, 97 (2000).

[48] W. S. B. Dwandaru, in *Numerical Study of the Totally Asymmetric Simple Exclusion Process that Consists of Only a Single Site for Modeling the Dynamics of Coulomb Blockade in 2D Quantum Dot*, AIP Conf. Proc. No. 1788 (AIP Publishing LLC, Melville, NY, 2017), p. 030070.

[49] A. John, A. Schadschneider, D. Chowdhury, and K. Nishinari, Traffic Like Collective Movement of Ants on Trails: Absence of a Jammed Phase, Phys. Rev. Lett. **102**, 108001 (2009).

[50] A. Kunwar, A. John, K. Nishinari, A. Schadschneider, and D. Chowdhury, Collective traffic-like movement of ants on a trail: Dynamical phases and phase transitions, J. Phys. Soc. Jpn. **73**, 2979 (2004).

[51] B. Schmittmann and R. K. P. Zia, Statistical mechanics of driven diffusive systems, Phase Transit. Crit. Phenom. **17**, 3 (1995).

[52] B. Schmittmann and R. K. P. Zia, Driven diffusive systems. An introduction and recent developments, Phys. Rep. **301**, 45 (1998).